



Universidad Autónoma de San Luis Potosí
Facultad de Ciencias



Coupled quantum wells as a novel source of optical anisotropies in nanostructured systems

Doctoral Thesis in Applied Sciences
submitted by:

Oscar Ruiz Cigarrillo

Supervisors:

Dr. Luis Felipe Lastras Martínez

Dr. Raul Eduardo Balderas Navarro

Dr. Edgar Armando Cerda Méndez

SAN LUIS POTOSÍ, S.L.P. MÉXICO
AUGUST 2022

Statement of authorship

I, Oscar Ruiz Cigarrillo, student of the Graduate Program in Applied Sciences of the School of Sciences of the Universidad Autonoma de San Luis Potosi, as author of the thesis "Coupled quantum wells as a novel source of optical anisotropies in nanostructured systems", declare that the thesis is an original, unpublished, authentic, personal work, that the corresponding sources have been cited and that in its execution the legal provisions in force that protect the copyright and intellectual and industrial property rights were respected. The ideas, doctrines, results and conclusions I have reached are my absolute responsibility.

Abstract

In the present work, it is proposed a new source of IOAs occurring in asymmetric coupled quantum wells ACQWs, namely a reduction of the symmetry from D_{2d} to C_{2v} as imposed by asymmetry along the growth direction. We report on reflectance anisotropy spectroscopy (RAS) of double GaAs quantum wells structures coupled by a thin (< 2 nm) tunneling barrier (CQWs). Two groups of DQWs systems were studied: one where both QWs have the same thickness (SCQWs) and another one where they have different thicknesses (ACQWs). RAS measures the in-plane optical anisotropies (IOAs) arising from the intermixing of the heavy- and light- holes in the valence band when the symmetry of the DQW system is lowered from D_{2d} to C_{2v} . If the CQWS are symmetric, residual IOAs stem from the asymmetry of the QW interfaces; for instance, associated to Ga segregation into the AlGaAs layer during the epitaxial growth process. In the case of an ACQWs with QWs with different thicknesses, the AlGaAs layers (that are sources of anisotropies) are not distributed symmetrically at both sides of the tunneling barrier. Thus, the system losses its inversion symmetry yielding an increase of the RAS strength. The RAS line shapes were compared with reflectance spectra in order to assess the heavy- and light- hole mixing induced by the symmetry breakdown. The energies of the optical transitions were calculated by numerically solving the one-dimensional Schrödinger equation using a finite-differences method. Our results are useful for interpretation of the transitions occurring in both, symmetric and asymmetric CQWs.

ACKNOWLEDGEMENT

CONTENTS

Abbreviations	III
List of codes and packages	IV
Symbols	V
List of Figures	VI
List of Tables	X
1 Experimental Details and Results	1
1.1 Samples Description	2
1.2 Spectroscopy: Experimental setups and results	5
1.2.1 Photoluminescence Spectroscopy (PL)	7

1.2.2	Photoreflectance spectroscopy (PR)	15
1.2.2.1	Excitonic effects	21
1.2.2.2	The PR summary	30
1.2.3	Reflectance Anisotropy Spectroscopy (RAS)	30
1.2.3.1	RAS strength discussion and the physical model justification	34
1.2.3.2	The RAS summary	38
	Bibliography	39

ABBREVIATIONS

BS	Band structure
BZ	<i>Brillouin zone</i>
QS	Quantum Structures
QW	Quantum Well
SQW	Single Quantum Well
CQWs	Coupled Quantum Wells
VB	Valence Band
CB	Conduction Band
SCQWs	Symmetric coupled quantum wells
ACQWs	Asymmetric coupled quantum wells
RAS	Reflectance Anisotropy Spectroscopy
PL	Photoluminescence spectroscopy
PR	Photoreflectance spectroscopy
R	Reflectance spectroscopy
PRD	Photo-Reflectance Differential Spectroscopy
FDM	Finite difference method
CCD	Charge coupled device
0D	Zero-dimensional
1D	One-dimensional
2D	Two-dimensional
3D	Three-dimensional
fcc	Face-centered cubic
2DEG	Two-dimensional electron gas
BL	Beer-Lambert-Law
TB	Tight-Binding method
PD	Photo-Detector
PEM	Photo-Elastic Modulator
QM	Quantum Mechanics
$k \cdot p$	Semiempirical theoretical tool to calculate band-structure
TB	Semiempirical Tight-Binding Method
DFT	Density Functional Theory
SOC	Spin-Orbit Coupling, also called Spin-Orbit interaction
LFLM	Dr. Luis Felipe Lastras Martinez group.
EFA	Envelope function Approximation
EMA	Effective Mass Approximation
FKOs	Franz Keldysh oscillations
IOA	In-plane Optical Anisotropy

LIST OF CODES AND PACKAGES

This list denote the *Open-Source* packages, codes, tools, and repositories for the development of this work. All inside of this work as images or numerical calculations are subject to the *Open-Source* ideology. Our codes are housed in our own GitHub repository, both personal and laboratory repository. It's important to say that without the development of the *Open-Source* codes like contents in this list, our codes, they couldn't be enhanced.

cqws-codes Repository of our codes implemented in this work. [1]

kp-lflm-group $k \cdot p$ julia [2] package developed by Our group research [3]

ASE The Atomic Simulation Environment (ASE) is a set of tools and Python modules for setting up, manipulating, running, visualizing and analyzing atomistic simulations. [4]

Spglib Software library for crystal symmetry search [5]

SOLCORE A multi-scale, Python-based library for modelling solar cells and semiconductor materials [6]

Aestimo One-dimensional (1D) self-consistent Schrödinger-Poisson solver for semiconductor heterostructures [7]

VESTA 3D visualization program for structural models, volumetric data such as electron/nuclear densities, and crystal morphologies. [8]

PGF/TikZ PGF is a macro package for creating graphics. It is platform- and format-independent and works together with the most important TeXbackend drivers, including pdfTeXand dvips. It comes with a user-friendly syntax layer called TikZ. [9]

pst-optexp PStricks package to drawing optical experimental setups. [10]

SYMBOLS

X⁻ Negative Trion

X⁺ Positive Trion

X Direct Exciton

IX Indirect Exciton

$\text{Al}_x\text{Ga}_{1-x}\text{As}$ AlGaAs semiconductor as a function of Al concentration x

\hbar Planck's constant (eV)

m_0 electron effective mass

(hkl) Family of lattice planes with Miller indices h , k and l

E_g Energy bandgap

e electron

hh heavy-hole

lh light-hole

$e_n - hh_n$ **or** $e_n - lh_n$ Electronic transitions

LIST OF FIGURES

1.1	GaAs substrate growth direction	2
1.2	AlGaAs superlattice	3
1.3	Processes that occur inside a solid in the light-matter interaction phenomena.	6
1.4	PL Scheme	8
1.5	Subfigure (a) shows PL experiments of the samples M4_3171 , M4_3172 and M4_3226 , where show spectra and results measured at 14K. Plots in how the comparison between these samples, where clearly can see the relative intensity among in each experiment. In (b) it can be seen each PL spectra with the respective direct transitions numerically calculated, hh1 and lh1 indicates the first energy level that corresponds to heavy- and light-holes respectively.	10
1.6	Absorption calculated as a function of sample depth, dashed lines closed the CQWs region, left: Figures 1.6(a) to 1.6(c),here the samples have $\text{Al}_x\text{Ga}_{1-x}\text{As}$ layers with different compositions $x = 0.15, x = 0.2$ and $x = 0.3$ this results in a change of refractive index then also expected in absorption. Right: Figures 1.6(d) to 1.6(f) these samples are equal in structure but change the width of one of the QWs, therefore the absorption manifests more homogenous than the first three samples.	12
1.7	(a) Shows the PL spectra to samples M4_3140, M4_3521 and M4_3523, in this comparison is clear the shift between these in respect to first transitions. The relative change in width of one of the QW modify the energy transitions being the sample 3521 the lowest energy. (b) It is plotted each PL spectra result with the correspondent e1-hh1 and e1-lh1m transitions energies.	13
1.8	Scheme of the PR effect where it shows the carrier dynamics, in left can see the photoinduced changes by the laser is applied.	16
1.9	PR Scheme	17
1.10	PR experiments to samples: M4_3171, M4_3172 and M4_3226 at 30K. Arrows point to calculated transitions for each sample, the used laser wavelength was the same, which in PL experiments and the power used in each of these was 5mW. Dashed line point the GaAs substrate.	18

1.11 PR experiments to samples: M4_3140, M4_3141, M4_3521, M4_3522 and M4_3523 at 30K. Arrows point to calculated transitions for each sample, the used laser wavelength was the same, which in PL experiments and the previous PR experiments. Dashed line indicate the GaAs substrate, in these samples this transition is well located. The PR spectra of sample M4_3522 p-type doped (orange) is five times smaller than their correspond n-type, the sample M4_3521. The experiments in sample M4_3140 was performed at 2.5mW, then was multiply it by four in according to samples M4_3521 and M4_3523, in case of the sample M4_3141 even if, was performed at a power = 5mW the result was 5 times smaller than sample M4_3521. The discussion about of this is explained in the text.	19
1.12 Comparison of : a) PR spectra of the 3521 (n-type) and 3522 (p-type) samples, the p-type sample is 5 times smaller than n-type sample. b) R spectra obtained at same time in each experiment, the arrows point to each direct transitions for two first confined energies. The line shape is practically the same in both spectra.	21
1.13 The PR comparison between samples M4_3521 (ACQWs-2) and M4_3523 (SCQWs), the electron wave function are plotted for each sample where, the SCQWs sample at top left and at top right to ACQWs sample. The top arrows pointed to forbidden transitions in ASQWs-1 sample, while the bottom arrows pointed to the direct transitions in both samples.	23
1.14 PR spectra of the ACQWs-1 sample designed as a function of slits aperture, where it can see the increase of peak resolution as decrease the aperture of slits.	24
1.15 The peak tends to height as increase the laser power, which also is very observable as a redshift.	25
1.16 Trions formation scheme in terms of band structure (a) in this case, the exciton is bound to an electron in the conduction band leading to a three-body system knew as negative trion \mathbf{X}^- . On the other hand, in (b) it presents the possible formation of \mathbf{X}^- due to a slight width of one in the CQWS, consequently, the narrow well transfers electrons through tunneling to a wide well, if it's calculated the wave functions of this structure, the wave functions have the characteristic of to be distributed asymmetrically as in the case of the applied electric field along z [11, 12].	26
1.17 Results to self-consistently Schrodinger-Poisson equation, in order with down to top the n-type layer $\text{Al}_{0.15}\text{Ga}_{0.85}\text{As}$ doped ($6 \times 10^{18}\text{cm}^{-3}$) is increasing in width from 15nm, 75nm, 150nm to 300nm. The goal of this is to calculate in a general way the effects of the dopped layer, specifically due to the electric field induced by this. The strength of the field is expressed in kVcm units, although this magnitude si great, we assume that doesn't significantly, latter we explained this.	28

1.18 Band conduction profile $V(z)$ calculated by numerical solution of self-consistent Schrödinger-Poisson equation. The calculations were performed considering the width of the doped n-type 6×10^{18} layer with 600nm. The zoom inset shows the comparison between total potential calculated (blue) and when applied field $F \approx 1.2 \text{ kVcm}^{-1}$ (dotted magenta), where at around of CQWs zone are similar.	29
1.19 RAS Scheme	31
1.20 Experimental results from samples: M4_3171, M4_3172 and M4_3226, from top to bottom respectively. In left, shows the RAS result where with a dashed line it's denote the substrate transition, in each sample denotes the direct transitions with arrows. The right side, show the plots of R spectra, which is the average result of all experiments carried in each correspond sample.	32
1.21 Experimental results from samples: M4_3140, M4_3141, M4_3521, M4_3522 and M4_3523, from top t bottom respectively. In left, shows the RAS result where with a dashed line it's denote the substrate transition, in each sample remarks the direct transitions with arrows. The right side, show the plots of the R spectra, which is the average result of all experiments carried in each correspond sample. Also, it's denote the RAS magnitude proportional to 7×10^{-4} , which in contrast with SCQWs samples the signal is smaller. The direct transitions it's locate by two peaks with opposite concavity where can see that the larger one transition is e ₁ -hh ₁ and smaller one associated with the e ₁ -lh ₁	33
1.22 RAS spectra for the (a), (b), asymmetric and (c) symmetric CQWs. The dashed vertical line indicates the expected energy of the excitonic transition of the GaAs substrate. Above this energy, the optical transitions come from the DQWs. The inset shows the PL spectra measured for each sample. Two peaks can be identified in each spectrum, a larger one associated with the transition e ₁ -hh ₁ and a much smaller one associated with the e ₁ -lh ₁ [for spectrum (b) this peak is observed as a shoulder]. The energies obtained from the PL spectra are indicated by the arrows in the RAS spectra. Note that the structures associated with e ₁ -hh ₁ and e ₁ -lh ₁ increase their strength when the DWQs become more asymmetric. The RAS spectra were measured at 30 K.	35

1.24 Reflection anisotropy (RAS, (a), (b)) and differential reflection (DR, solid line) spectra for ACCQWs-2 and ACQWs-3, grown on an AlGaAs n-type and p-type layer respectively. Note that while for the heavy hole transitions (e1-hh1 and e2-hh2) in the RAS and DR spectra have the same concavity, for light holes transitions (e1-lh1 and e2-lh2) the concavities are opposite and DR spectra shows the highest level transitions. The bottom arrows point to the experimental transitions for the two first levels, whereas the top arrows show the calculated energies to three energy levels. The RAS and DR spectra were measured at 30K.	36
1.26 RAS experiment designed to demonstrate the non-existence of built-in electric field trough sequential measured along the preferential direction, in this case, it was chosen along the pits [1 $\bar{1}$ 0] [13]. The signal result in both samples practically is the same, the sign is conserving. At top left and right located the images taken with a microscope of back substrate which shows the pit reveals along of [1 $\bar{1}$ 0] direction.	38

LIST OF TABLES

1.1	Table of samples description	4
1.2	Photo-cathodes,usually implemented in PD to the spectroscopy of semiconductors [14].	7
1.3	Table of PL experimental parameters	9
1.4	Comparison table between experimental transitions obtained trough PL measures and numerical transitions calculated as explained in ??	14
1.5	Comparative of experimental (E) and numerical calculations (N) of first level transition energies (in eV). δE_e , δE_{hh} and δE_{lh} corresponds to the difference between electrons, heavy- light holes states, respectively. ΔE_n is the numerical calculation of energy splitting for transitions 1 and 2 (n = 1, 2).	36

1

EXPERIMENTAL DETAILS AND RESULTS

This chapter shows the experimental results in the spectroscopy detailed in it which are compared and correlated among them, to success a physical explanation of the obtained results.

Contents

1.1 Samples Description	2
1.2 Spectroscopy: Experimental setups and results	5
1.2.1 Photoluminescence Spectroscopy (PL)	7
1.2.2 Photoreflectance spectroscopy (PR)	15
1.2.2.1 Excitonic effects	21
1.2.2.2 The PR summary	30
1.2.3 Reflectance Anisotropy Spectroscopy (RAS)	30
1.2.3.1 RAS strength discussion and the physical model justification	34
1.2.3.2 The RAS summary	38

1.1 Samples Description

QUANTUM STRUCTURES were created thanks to the technic Molecular Beam Epitaxy (MBE) growth which in general terms consist in great precision of the growing thin films of semiconductor materials, through high precision deposition on a suitable crystalline substrate. As has been pointed out on many occasions, MBE is nothing more than a sophisticated form of vacuum evaporation* [15], this does not sound bad but the MBE technique is not only this, epitaxial growth needed the precision in experimental growth parameters how temperature, deposition rate calculations, REED analysis, etc. So that in a bit of words the purpose is to supply appropriate atoms or molecules to the substrate surface and leave surface diffusion, surface reactions and inevitable desorption from the surface to play their various roles in generating an epitaxial film [15, 16].

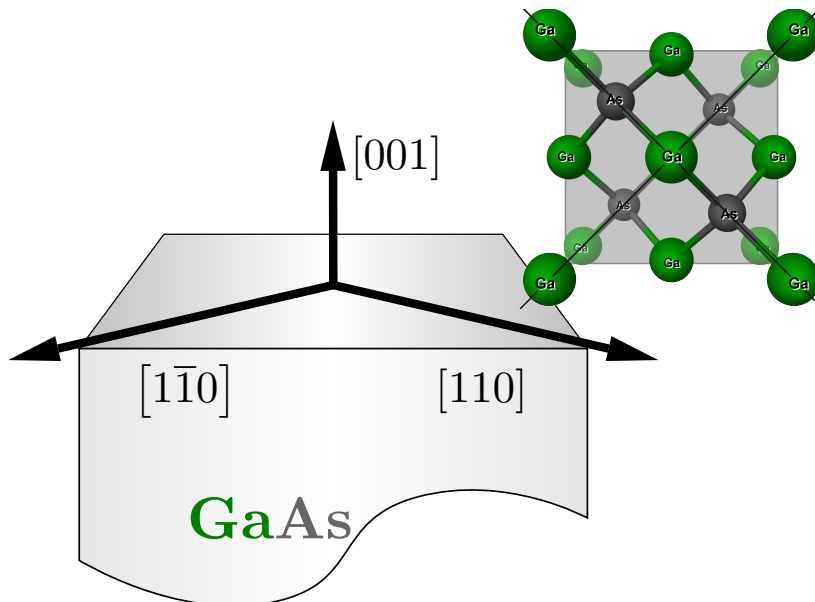


Figure 1.1: GaAs substrate

The samples studied in this work, are made up of a GaAs (001) substrate, the GaAs substrate has a zincblende-type crystal structure, in which the atoms are tetrahedrally coordinated. Figure 1.1 the choice of crystal is very important and preparation of these can modify the growth result, for this reason, the high quality of substrate is the basis of growth of heterostructures. The heterostructures are a combination of more than one semiconductor, this leads to the superlattice definition where more of two semiconductors are

*In owner experience, MBE growth is a very exhausting task, so great respect to all people that works on this

atomically deposited over the substrate in the growth direction (001). The semiconductors used in the samples are GaAs and AlAs then these can have different thicknesses, growing periodicashowgrid][lly and alternately way over the substrate with thickness $d_{\text{GaAs}} + d_{\text{AlAs}}$. The result consists in an arrangement of $(\text{GaAs})_2(\text{AlAs})_2$ superlattice, like a shown in Figure 1.2 or AB arrangement like a said commonly. In QWs structures, the width is the principal characteristic because quantum confinement is dependent on this, then MBE is the perfect choice to realize this.

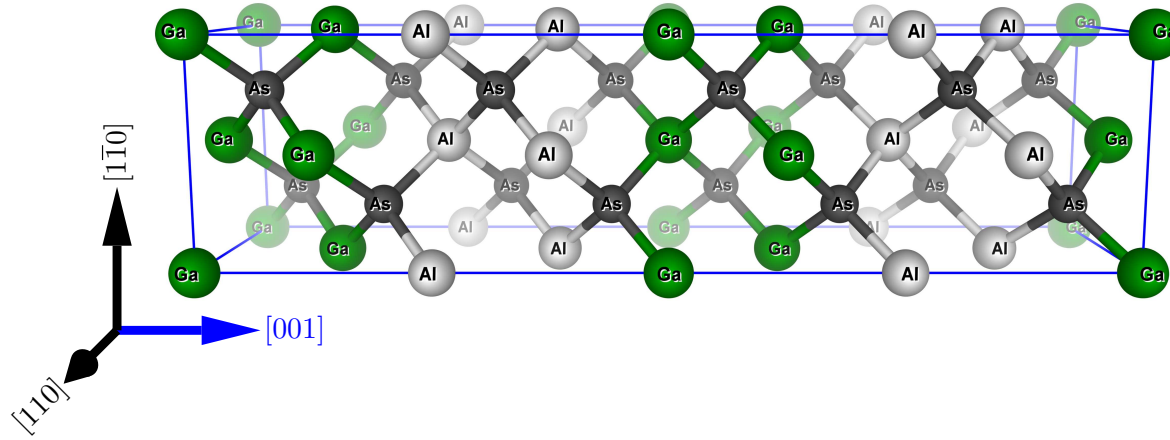


Figure 1.2: Atomic order in AlGaAs crystal structure grown along (001) direction.

The realistic structures present some details that can modify the experimental results, some of these are inevitability due to the complexity of growth. One of these is the interfaces between two different materials, i.e., the typical structure of GaAs/AlGaAs has an interface between these, then the problem is due to an imperfect mismatch of materials, therefore, can cause anisotropy effects. Other details which usually are considered are surface, point defects along of structure, or strained caused by overlayer in the epitaxial process. Later, the interfacial detail gives the physical sense to RAS experiments in the symmetric CQWs structures.

Table 1.1 shows the sample names, each sample has two QWs coupled by a thin barrier preferentially of $\text{Al}_x\text{Ga}_{1-x}\text{As}$ semiconductor where Al percent is important because of the barriers potentials depends on this, in the case of AlAs barriers the potential barrier is bigger than $\text{Al}_x\text{Ga}_{1-x}\text{As}$. As a before-mentioned, this was taken into account in numerical calculations to generate the potential profile. Commonly for the case, $\text{Al}_x\text{Ga}_{1-x}\text{As}$ barriers both in adjacent like the coupling barrier the x values are in the interval $0.1 < x < 0.4$.

1.1. Samples Description

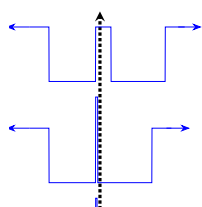
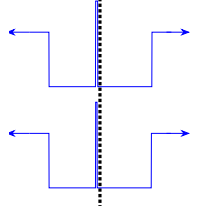
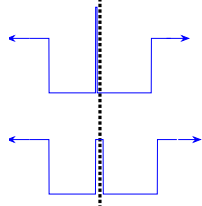
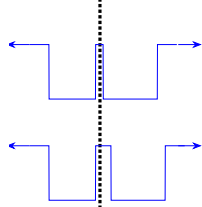
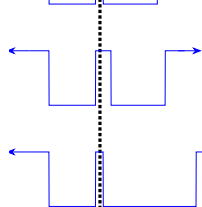
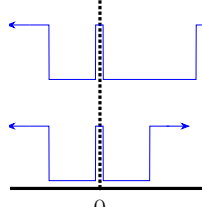
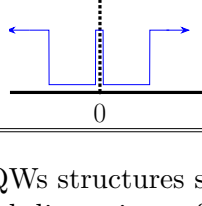
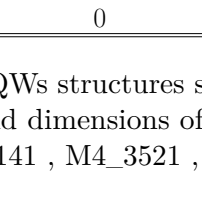
Sample	NW width (nm)	$V(z)$	WW width (nm)	Barrier width (nm)	Barrier	Adjacent barriers	Doped type	$\left[\frac{1}{cm^3} \right]$
M4_3171	11.87		13.85	3.960	AlGaAs	Al _{0.15} Ga _{0.85} As	n[Si]-i-n[Si]	6×10^{18}
M4_3172	11.87		13.85	0.565	AlAs	Al _{0.30} Ga _{0.70} As	n[Si]-i-n[Si]	6×10^{18}
M4_3226	11.87		13.85	0.424	AlAs	Al _{0.30} Ga _{0.70} As	n[Si]-i-n[Si]	6×10^{18}
M4_3140 (ACQWs-1)	11.87		13.85	1.980	AlGaAs	Al _{0.15} Ga _{0.85} As	i-n[Si]	6×10^{18}
M4_3141	11.87		13.85	3.960	AlGaAs	Al _{0.15} Ga _{0.85} As	i-n[Si]	6×10^{18}
M4_3521 (ACQWs-2)	11.87		23.74	1.980	AlGaAs	Al _{0.15} Ga _{0.85} As	i-n[Si]	6×10^{18}
M4_3522 (ACQWs-3)	11.87		23.74	1.980	AlGaAs	Al _{0.15} Ga _{0.85} As	i-p[Be]	5×10^{16}
M4_3523 (SCQWs)	11.87		11.87	1.980	AlGaAs	Al _{0.15} Ga _{0.85} As	i-n[Si]	6×10^{18}

Table 1.1: This table shows the CQWs structures studied in this work. CQWs potential profiles $V(z)$ are shown to observe the different shapes, composition parameters, and dimensions of structures studied. The dashed line determines the symmetric reference in the last samples in which we focused (M4_3141 , M4_3521 , M4_3522 , M4_3523), due to their characteristic results.

Worth mentioning that the purpose of the first four samples (up to down in table) they were grown with the objective of measure indirect excitons (IX), so that, the structures are more complex, and we omitted the value of n-doped since these samples are doping in bottom and top to minimize the intrinsic electric field (screening field effect) so that external perturbation is applied through a voltage over the sample [17] and the n-doped enhance the external perturbation *.

After realized experiments over the four first samples and observe possible trions (X^+ or X^-) through PR spectroscopy and an apparent increase of the RAS signal, it was decided to focus the experiments on these structures, which have a less complex composition as in the case of the first three samples in the table (see Table 1.1). Therefore, it took the sample M4_3141 as a basis, i.e., same barriers widths both coupling barrier and adjacent barriers, obtained the samples M4_3521 , M4_3522 and M4_3523 where sample M4_3522 is the same to sample M4_3521 in structure but with a different type of doping (p-type in M4_3522 and n-type in M4_3521), samples M4_3521 and M4_3522 have the same doping type (n-type in both) but one of the QW is more width to another, this means that the sample M4_3523 have the same thickness in both QWs (SCQWs) and sample M4_3521 have one QW thick more than the another (ACQWs).

The Section 1.2 shows each experimental setup implemented in this investigation with their respective results. Starting with the Section 1.2.1 shows PL spectroscopy, their experimental setup implemented to obtain transitions energies values and compare with numerical results, after, in Section 1.2.2 shown experimental setup and results of the PR spectroscopy, to get information about the intrinsic electric field and the effects caused by this. Finally, Section 1.2.3 shows the RAS experimental setup and exposes the experiments that were realized to study the anisotropy caused by the asymmetry due to the relative thickness between the CQWs.

1.2

Spectroscopy: Experimental setups and results

OPTICAL SPECTROSCOPY frequently is defined as a branch of physics that studies the *light-matter interaction*, this is important because the simple definition of interaction covers a vast realm of physical phenomena from classical to quantum electrodynamics [18]. Therefore, optical spectroscopy is an essential tool in experimental solid state physics, gives the guide to study optical and electronic properties of semiconductors.

The optical process in semiconductors consists of the study of response due to *light-matter*

*Non-published, the specific information about the doped in these growths, if you have a question about this, you can send email to Dr. Klaus Biermann biermann@pdi-berlin.de

interaction, this response corresponds basically to the processes that can occur in the solids when light* falls on (photons) in it. These processes are absorption, reflectance, emission, and scatter where all of this depends on electromagnetic spectra range, in our case this range includes from near-infrared to mid-infrared (700nm to 900nm). Although those processes are of the utmost importance, optical spectroscopies that uses in this work involve more interest in absorption and emission, being the latter sensed in our experimental setups.

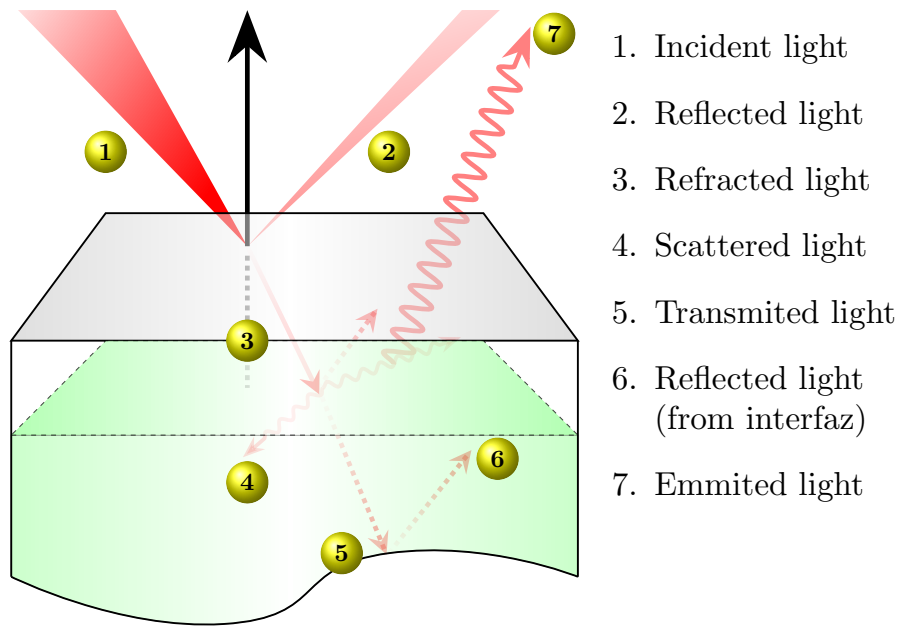


Figure 1.3: Processes that occur inside a solid in the light-matter interaction phenomena.

Before continuing with the manuscript of this chapter, I would like to mention that the experiments could not be carried out without the development of detectors, specifically optical detectors. To speak about optical detectors, it is impossible not to mention the photoelectric effect that in general terms is the transfer of energy from photons to electrons when the light spot on a surface [19]. So, this fundamental quantum phenomenon is the basis of detectors in spectroscopy, these detectors are called photodetectors, where these convert the light power(photon incidence over their sense area) into an electric signal, voltage, or current, then this signal we can measure and amplify it. The next sections will mention and discuss the PD implemented in the experimental setup and especially which are the pros and cons. It is important that the photo-cathode of the photo-detector corresponds to the spectral range of experiments. i.e, in our experiments the spectral range of interest is from 700nm to 900nm the PD should have characteristics to adequate of this range. The Table 1.2 shows some PD and their characteristics [14].

As a comment, it is important to denote that the CCD devices are been span in many

*Refers to light due to radiation spectral range

Cathode	Range (nm)	$\phi(\%)$	$\lambda(\text{nm})$	$i_d \text{ nA}$
bialkali (S-22)	300-630	26	400	0.1
multialkali (S-20)	180-800	20	480	0.2
extended red multialkali (S-25)	300-900	7	600	1
GaAs	300-920	15	700	2
Cs-Te	160-320	14	200	0.01

Table 1.2: Photo-cathodes, usually implemented in PD to the spectroscopy of semiconductors [14].

setups in recent years and this is because these devices enlarged the range of experiments that can be realized with these, above all in other areas of physics as in the experimental astrophysics in which has obtained awfully important results. Nowadays, CCD devices in experimental solid-state physics have contributed to getting great experiments that previously were limited due to spatial resolution and time response. In the section 1.2.1, it discusses the advantages and cons of the detectors (PD and CCD) in PL spectroscopy context.

1.2.1 Photoluminescence Spectroscopy (PL)

Photoluminescence spectroscopy is characterized by be a fast spectroscopy to get optical properties (i.e band-gap) and transitions in semiconductor materials, for this reason the work began with PL spectroscopy with aim of searching optical transitions in each CQWs samples and compare with numerical solution of one-dimensional Schrödinger equation (see ??).

Although PL signal is characterized by be greater than other spectroscopies implemented in this work, the need to use a chopper is only to filter the signal to the external noise, this is achieved used a lock-in amplifier where the reference signal is the chopper and signal input is first measured by a multimeter and then input in the lock-in amplifier. In many other experimental setups the experimental measure are take fast, this is because implement a CCD device as a detector of experimental signals, where these devices are distinguished by fast time of acquisition (apart from other reasons). In our case the time of measure it does not comparable with those, due the time in our experiments is about 2 hours (explained latter) and those are about several minutes. But why use lock-in amplifier if CCD devices shorter measured time?

The answer is not be for impatient*, the reason is that, the lock-in and detector implementation allow control over spectral resolution through two parameters, the first one is in the choice of monochromator's slits apertures and the second one has to do with step

*The author self-considered impatient

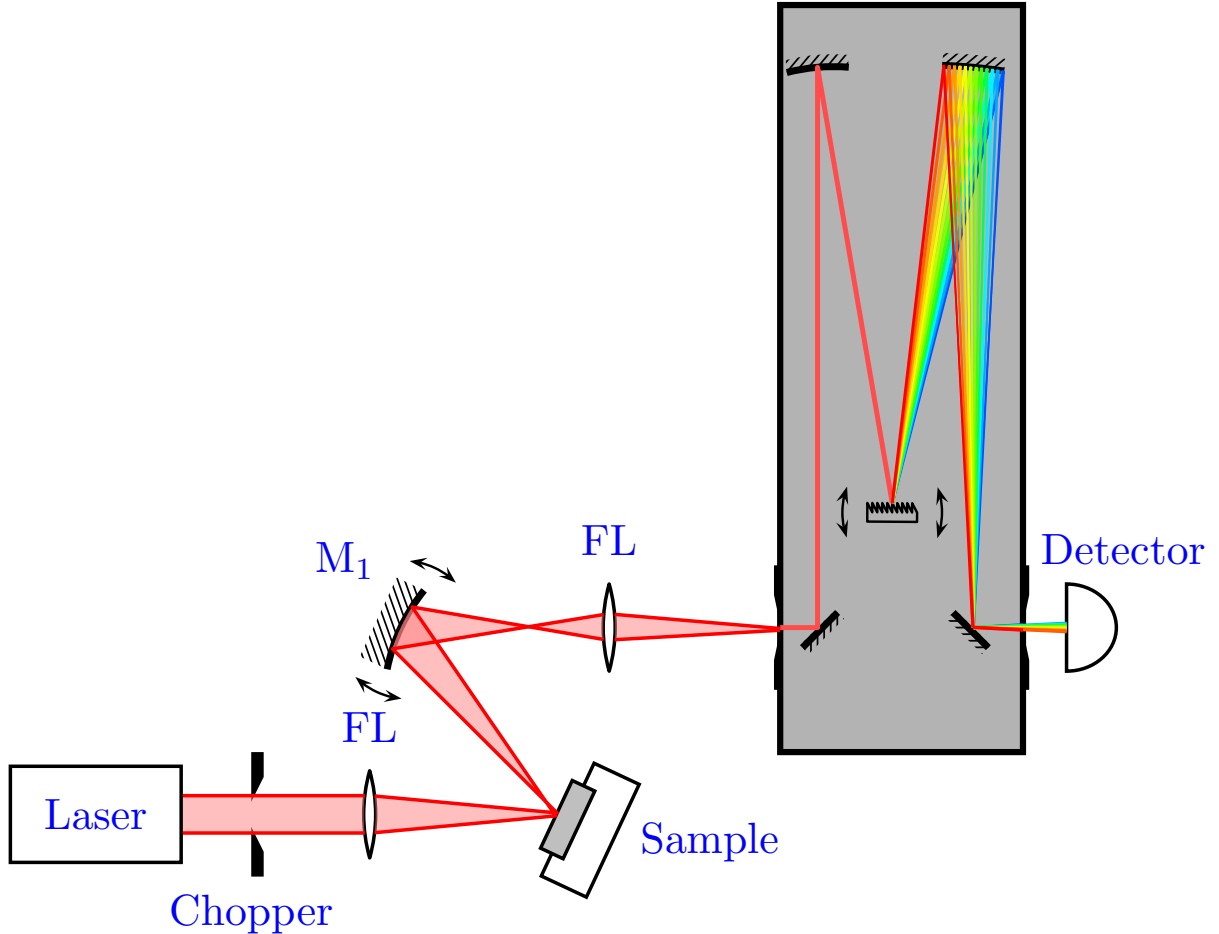


Figure 1.4: Scheme of photoluminiscense setup, the temperature of experiments at 14 K, the wavelength of laser 685nm and was used a Si detector.

wavelength this is the progress step by step over the spectral range taking into account in the experimental measure. Also, the step by step experiments provide the choice of measures number in each step where finally only consider the average of these points, resulting more clean spectra in compare with CCD setups*. Although the time is important worth it inverts to get quality experiments.

Some experiments shown below correspond to Carlos's bachelor thesis [20], who implemented a simple and reliable PL system also he makes a computational code to fit PL spectra using numerical and experimental results (you can check Carlos's codes in our laboratory repository on GitHub[†]). These results were correlated with previously realized experiments taking into account the same parameters.

The experiments are organized by labels, how shows in Table 1.1, started with the samples

*Even if modify time and average of measures, the spectra measured with lock-in amplifier are more quality.

[†]<https://github.com/Spectroscopies-Lab-IICO>

M4_3171 , M4_3172 and M4_3226 where these samples were grown with objective the measure trions. The experimental parameters are shown in Table 1.3, in each experiment the optical setup was optimized to enhance the signal measured, the optimization process consisted in measure laser peak at a definite monochromator slit's aperture then finely move the mirror until achieving a high response in multimeter, repeat this closing the slit's and measuring the FWHM of the laser peak in each step, finally we obtained an optimal resolution about 1 nm in our PL experiments.

Sample	Laser	Range(nm)	λ step (nm)	No. of singnal acquisition	Slits aperature (μm)
M4_3171	680	800-820	0.1	20	75
M4_3172	680	780-840	0.1	15	75
M4_3226	680	800-820	0.1	20	100
M4_3140	680	800-820	0.1	20	100
M4_3141	680	800-820	0.1	20	100
M4_3521	680	800-820	0.1	20	100
M4_3522	680	800-820	0.1	20	100
M4_3523	680	800-820	0.1	20	100

Table 1.3: PL experimental parameters implemented in each sample, all experiments were carried about 14K and was used the same red (680 nm) laser diode. The measured parameters as a Wavelength step or number of acquisitions per step Wavelength were optimized as explains in the text.

An important detail about module laser ThorLabs and very remarkable in the Section 1.2.2 is related to power, the power of this was not stable in some time periods causing a variation in the results, this is the reason to use different experimental parameters and after some test were optimized the choice of the Wavelength step, number of acquisitions per λ step and slits aperture, this depending on each sample.

The PL spectra, corresponding to the samples showing in Figures 1.5(a) and 1.5(b), were more complicated to interpret and in experimental conditions as well. For this reason, we decided to calculate the absorption along of the structure that composes each sample because due to they have more layers. We speculated that this is the reason why it was complex to realize the experiments and their analysis. As previously spoken, the study of light-matter interaction in solids can be a headache this is because in real experiments more than one interaction mechanism can be observed, especially in PL spectroscopy and, the objective is to measure only one of them, therefore, the experimental results can be affected and complicate their interpretation. The reason for starting with the samples of Figure 1.5 is that they have effects that modify the PL spectra and, although these effects are very interested in our case, they reduce the PL signal.

If started with the scoop, that the PL spectrum in semiconductors is given by an interband emission generated by recombination carriers, and this, in turn, is due to the absorption

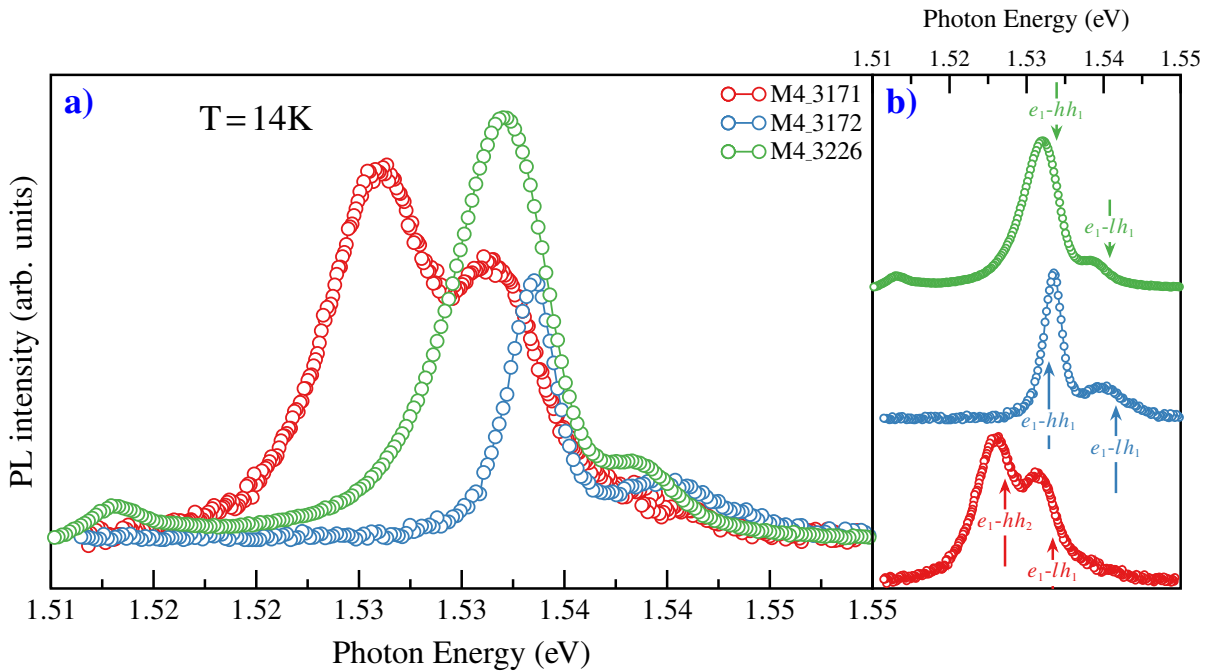


Figure 1.5: Subfigure (a) shows PL experiments of the samples M4_3171 , M4_3172 and M4_3226 , where show spectra and results measured at 14K. Plots in how the comparison between these samples, where clearly can see the relative intensity among in each experiment. In (b) it can be seen each PL spectra with the respective direct transitions numerically calculated, hh1 and lh1 indicates the first energy level that corresponds to heavy- and light-holes respectively.

of photons provided by an excitation laser source. Therefore, the PL signal is due to absorption, it does not matter that they are opposite processes, the absorption, as well as many other mechanisms of light through the solid, can modify and generate the spectrum of PL. The absorption analysis was carried on in the macroscopic approach to light-matter interaction (in ??, talks about quantum processes and aspects of light-matter interaction in a microscopic environment), therefore, can use classical electrodynamics to study optical properties of semiconductors. One crucial property of semiconductors is the dielectric function, this is proportional to the complex refractive index (later it is named only as refractive index) and with this, can be described the optical properties of semiconductors. It is important to mention that the refractive index describes how light propagates in a medium, and it expressed as [21, 22]:

$$\tilde{n} = n + i\kappa = \sqrt{\varepsilon(\omega)} \quad (1.1)$$

where the real part (n) represents the refractive index and the imaginary part (κ) is the extinction coefficient. Even if the objective of this work does not rewrite and reinterpret the physics of these phenomena, we will try to focus on specific equations to reach the

goal, which is the absorption model in semiconductors. Then the electric field inside a solid can be written as [22–24]:

$$\mathbf{E} = \mathbf{E}_0 \exp\left(\frac{-\kappa\omega z}{c}\right) \exp\left(-i\omega\left(\frac{nz}{c} - t\right)\right). \quad (1.2)$$

In the Equation (1.2), we can see the solution of Maxwell equation in a macroscopic picture of the photon-material interactions. This represents a wave propagating with dispersion and staying in terms of refractive index, but the principal idea is to establish a relationship that can help us to describe the absorption in terms of these principal parameters. The absorption is a process that occurs in any spectroscopy and is the absorption coefficient that defines such a feature in each medium. The extinction coefficient κ is the cause of the wave damping when the electromagnetic wave crosses in media, therefore it's related by absorption coefficient. Now in Figure 1.3 we can see that there are three principal parts, that they are intensities that are reflected, transmitted, and absorbed. These three parts compose the original incident light through:

$$I_0 = I_R + I_T + I_A \quad (1.3)$$

Finally, we call upon one of the most notable laws in spectroscopy, this basic expression relates the intensity of light absorbed with the absorption coefficient and is known as Beer-Lambert law [25, 26]:

$$I(z) = I_0 \cdot e^{-\alpha z}, \quad (1.4)$$

then this tells us how intensity decreases as a function of absorption coefficient. As a result of these basic principles in a real structure, we can define absorption in each layer. After these general and quick basics of the macroscopic basis of light-matter interaction, let's move to a more realistic environment where the calculations are more complex and where it is decided that parameters have major physical priority. The numerical solutions of absorption along structure were carried out using an exceptional Open-Source code called **SOLCORE** [6]* and our codes. As previously mentioned in a real calculation is frequently taken into account only parameters with major physical sense depending on the situation, arduous computational solutions, or for simplicity. From **SOLCORE**, we have the simplest model to calculate the absorption, despising all reflections at the interfaces having only the absorption as a function of wavelength and depth z expressed as:

$$A_n(\lambda, z) = \alpha_n(\lambda) \exp\left(-\sum_{i=1}^{n-1} \alpha_i(\lambda) d_i - \alpha_n(\lambda)(z - z_n)\right) \quad (1.5)$$

*You can test and contribute this code, visiting their GitHub repository at <https://github.com/qpv-research-group/solcore5.git>.

where α_n is the absorption of layer n , d_i is the thickness and z_n the position of beginning of the layer*.

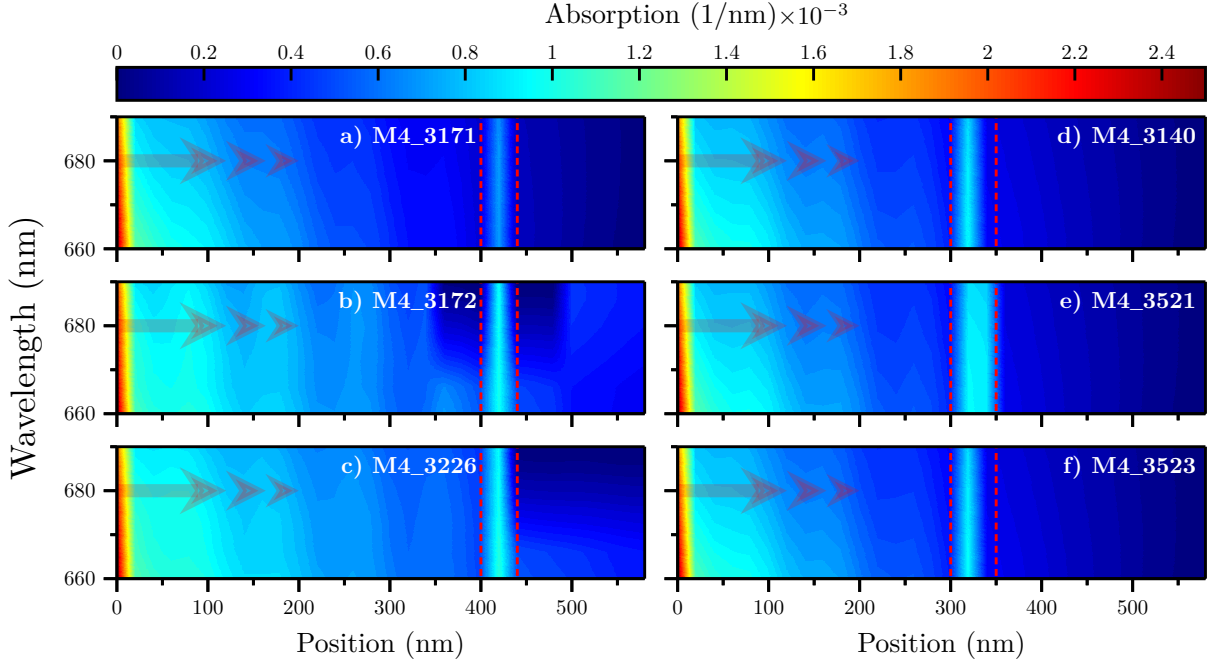


Figure 1.6: Absorption calculated as a function of sample depth, dashed lines closed the CQWs region, left: Figures 1.6(a) to 1.6(c), here the samples have $\text{Al}_x\text{Ga}_{1-x}\text{As}$ layers with different compositions $x = 0.15, x = 0.2$ and $x = 0.3$ this results in a change of refractive index then also expected in absorption. Right: Figures 1.6(d) to 1.6(f) these samples are equal in structure but change the width of one oM4a)f the QWs, therefore the absorption manifests more homogenous than the first three samples.

The samples with extra layers have characteristics that don't present in samples with fewer layers, one of this is which the fundamental transition around the GaAs gap doesn't possible to observe in these samples, the amplitude in these samples in comparison with sample M4_3141 for example, is around of twenty times smaller than this, opposite case in samples M4_3140, M4_3421, M4_3523. We take these samples because these are the basis of this work, the complete set of PL experiments corresponds to the work previously mentioned. So, why is the important to get the PL results and calculate absorption? The answers are simple, the importance to get PL spectra to help us to get experimentally energy transitions, which have a very important role in the next experiments and in the basis of our model to explain the increase in anisotropy in the ACQWs. Also, the experimental PL results are the basis to compare that our numerical calculations are consistent with the experiments. Numerical calculations get more complicated in large structures, this means, while the structure is conformed with more layers and these layers

*In eq. (1.5) originally the thickness is represented how w_i , by confusion issues it was decided to change the notation.

are thicker, the probability to get a divergence in calculations is great, this is the reason which not all models work. In fact, in our numerical calculations the energy transitions in samples with more layers (M4_3171, M4_3172, M4_3226) we had to be careful at the moment to choice energy binding, the reasons are many and in the PL is complicated to get unique information and even less in structures with high doped, the charge recombination they play us dirty to understand the results.

The case of absorption calculations is a guide to explain the difficulty to carried out PL experiments and put to discussion if doping is a reason to generate or not intrinsic electric field, after all the absorption is part of field solutions.

Figures 1.6(a) to 1.6(c) are the calculations of absorptions as a function of depth, where previously explained, it was only taken into account classical regime therefore the absorption remains in terms of the optical parameters of each layer which conforms all structure. In these figures can shows that in a range of 650 nm to 700 nm the wavelengths are absorbed with major proportion in the first layer, this is due to the structures starts with a GaAs doped(n- or p-type) or undoped layer. After along in structures, also can observe the decrease absorption to short wavelengths, and the notably increased around of the coupled quantum wells.

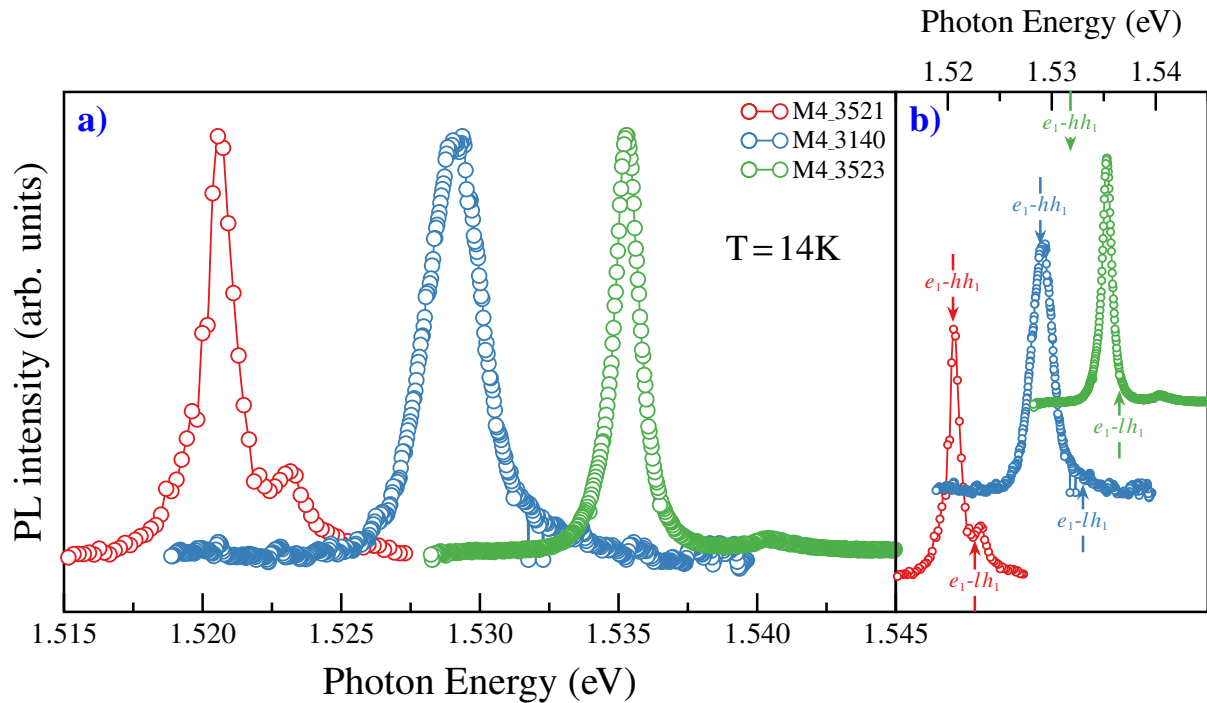


Figure 1.7: (a) Shows the PL spectra to samples M4_3140, M4_3521 and M4_3523, in this comparison is clear the shift between these in respect to first transitions. The relative change in width of one of the QW modify the energy transitions being the sample 3521 the lowest energy. (b) It is plotted each PL spectra result with the correspondent $e_1\text{-}hh_1$ and $e_1\text{-}lh_1$ transitions energies.

These calculations make sense in the next section where PR spectroscopy is a powerful tool that can be used to measure the optical properties due to the modulation without external perturbation, this means that the modulation depends on the intrinsic properties of the structure. The generalizability of the results is limited by the classical regime, as previously mentioned, it has taken into account the refractive index where the absorption can obtain from the complex part of this, that is the extinction coefficient. The common use of the PL is to determine the band gap and optical transitions in semiconductors, especially in QS as quantum wells, but what happens if consider PL regardless of the penetration depth? In our case it is important doesn't, due to the structures studied have wide layers before of coupled quantum wells region, this can observe in figure 4 where shows the results of samples: M4_3171, M4_3172, M4_3226, M4_3140, M4_3521, and M4_3523. In the PL experiments carried out here, it was used as a show in Figure 1.4 a red laser diode of $\lambda = 685$ nm, although the laser energy is chosen in respect to energy gap therefore short wavelengths are preferable but how we can see these wavelengths are absorbed in the first layer due to the samples ends in a GaAs layer, even the laser used is absorbed in large proportion.

Contrary to the samples measured first, the samples M4_3140, M4_3521, and M4_3526 exhibits the most spectral resolution this means that exhibit a more homogenous behavior due to the QWs have quantized energy, therefore, the electron-hole recombination is more probably to measure than the other samples which present width spectrums so that these results may be due to the several internal mechanisms of which can be: impurities, large carrier density due doped, defects, among others [27, 28]. In each of these PL spectra, Figures 1.5 and 1.7 present the most intense peaks associates with heavy- and light-holes exciton transitions denoted by e1-hh1 and e1-lh1 respectively.

Transition		M4_3171	M4_3172	M4_3226	M4_3140	M4_3521	M4_3523
e1-hh1	(E)	1.5270	1.5341	1.5329	1.5170	1.5207	1.5354
	(N)	1.5313	1.5342	1.5339	1.5292	1.5196	1.5354
e1-lh1	(E)	1.5318	1.5402	1.5286		1.5234	1.5406
	(N)	1.5370	1.5414	1.5408	1.5335	1.5220	1.5366

Table 1.4: Comparison table between experimental transitions obtained through PL measures and numerical transitions calculated as explained in ??

In discussion with the before mentioned mentioned, several mechanisms can contribute to getting an inhomogeneous spectrum, even it can say that the two peaks which correspond to exciton transitions are thick and merge this can be related with the high doped level this is because very high dopant concentration causes an overlap of the impurity band with the free-carrier continuum [28]. Table 5 shows the comparison between experimental transitions energies get with PL and the numerical results. It is important to mentioned

that the approximation of numerical calculations are closed to experimental, the difference is about of 5 meV for the PL case. It is well-known that the PL signal is increase as a function of decrease well widths, as shows

Table 1.4 shows the comparison between experimental transitions energies get with PL and the numerical results. It is important to mention that the approximation of numerical calculations is closed to experimental, the difference is about 5 meV for the PL case. It is well-known that the PL signal is increased as a function of decrease well widths, this due to the energy of the confined particle state depends on strongly in it and this is demonstrated in Figure 1.7 this due to structures doesn't have top n-type epitaxial layer these structures are i-n type, staying only barriers structures and PL line shape presents strong confinement [29–31].

1.2.2 Photoreflectance spectroscopy (PR)

POTOREFLECTANCE belongs to the group of modulation spectroscopy, being one of the most important to determines field effects without external perturbations, this means that there is no need for an external source that generates the electric field on the sample. Exists another's kinds of modulation spectroscopy, where the type of modulation depends on interest effects, these can be phenomena linked with temperature (thermoreflectance), strain (piezoreflectance), electric (electroreflectance), etc. There is a great information amount of based on this technique, so it decides as previously mentioned and not to repeat in future chapters or sections, the principal idea is to focus on more representative expressions and phenomenological interpretation which be the best following our models and results. Unlike the PL the PR is the reflectance measure as a function of modulation or the changes in it, this once more needs to involve optical properties of the sample studied, in the eq. (1.1) is expressed the refractive index with their real and imaginary part respectively and these are proportional to dielectric function. If the PR is the change in R which is due to modulation of an intrinsic electric field generated by doped layer o layers in the sample (later discuss this mechanism) this mean that:

$$\frac{\Delta R}{R} = \frac{R_{\text{off}} - R_{\text{on}}}{R_{\text{off}}} \quad (1.6)$$

where R_{off} and R_{on} are the reflectivity when the perturbation (laser) are activate or not are the reflectivity when the perturbation (laser) are activated or not, this mean that the results falls on perturbation that is the laser.

The PR as modulation spectroscopy is a powerful tool to perform the study of semiconductors, their modulation mechanism occurs when the built-in field is screening by photoexcited carriers created through incident photons, which involves contactless and

non-destructive. In many cases, this spectroscopy technique is preferred due to it can measure transitions in heterostructures at room temperature in comparison with the PL or PLE [32] that are measured at low temperature. Therefore, the highlighter characterize of the PR is the modulation of the built-in electric field, in part, this is due to the structure characteristics but in fact, the PR spectra is the change that generated electric field in the dielectric function, this is expected because is the result of measured the changes in reflectivity generated by the laser, in other words, the laser induces an excess of carriers which neutralize intrinsic field. This is well-known to study in the bulk materials, the models show as the reflectivity change is very well approximated by a first-derivative [33–36] but in QWs structures that are dominates by excitonic transitions then the PR line shapes can be understood in terms of modulation of dielectric function appropriate for excitons [32, 37–39].

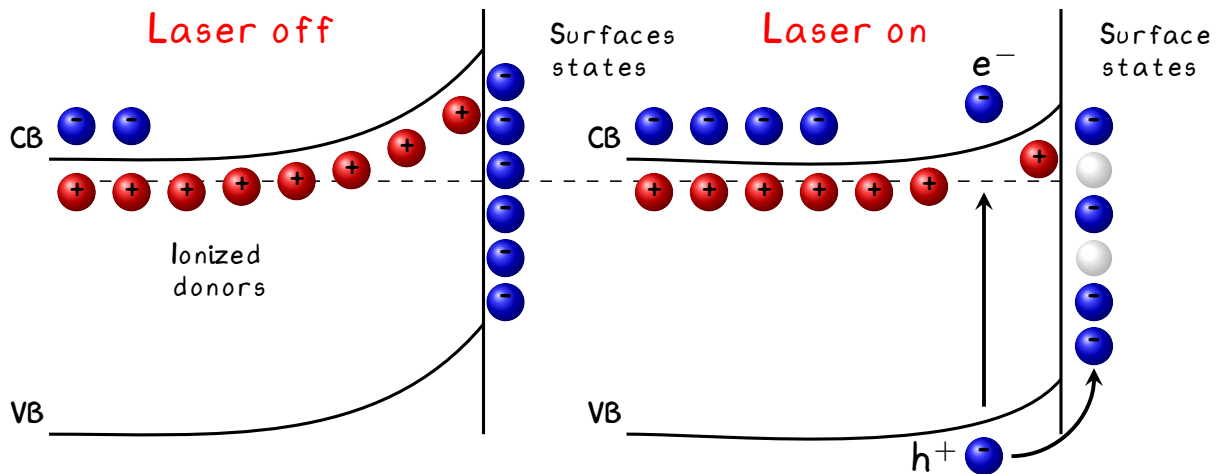


Figure 1.8: Scheme of the PR effect where it shows the carrier dynamics, in left can see the photoinduced changes by the laser is applied.

Under the objective of this thesis, we have not focused on doing a traditional study of the line shape with their respective model, the study over PR lineshape is complex, the interpretation starting from changes in dielectric function like a derivative shape and depending on magnitude perturbation, i.e, doesn't is same the PR analysis on structures with free carriers in solid that the confine particles in QWs structures, the bounded particles are not accelerated by built-in field modulation, so the energy spectrum is discrete and not continuous like free particles. The capability to implement a lineshape fit, do the PR be a great tool. It has been mentioned which the photoreflectance process is due to the built-in electric field modulation, therefore we are considering that the sample was grown considering desired characteristics to generate an intrinsic field, this means that sample contains n-type doped layers, impurities, unintentional strain mechanisms which generate a space charge region. In the case of an n-type doped layer in a structure, create a space charge region, this region creates the field therefore the conduction and valence bands are bending as a show in the Figure 1.8 and the Fermi energy are pinning at the surface.

Photoexcited electron-hole pairs are separated by the built-in field, with the minority carrier (holes in this case) being swept towards the surface.

At the surface, the holes neutralize the trapped charge, reducing the built-in field [35]. That is the general explanation to the PR modulation, before we mentioned that a characteristic of the PR, is to fit as a derivative-like and the order depends on structure, also, we mentioned which in quantum wells the confinement and bound states modify the line shape and the respective fit. So, in this situation, the modulation of field causes the binding energy change of excitons, in other words, this is a Stark effect but in an inverse case because of the field it already exists. The electron-hole pairs depend on binding energy, if that is modified, then the intensity of the transition varies.

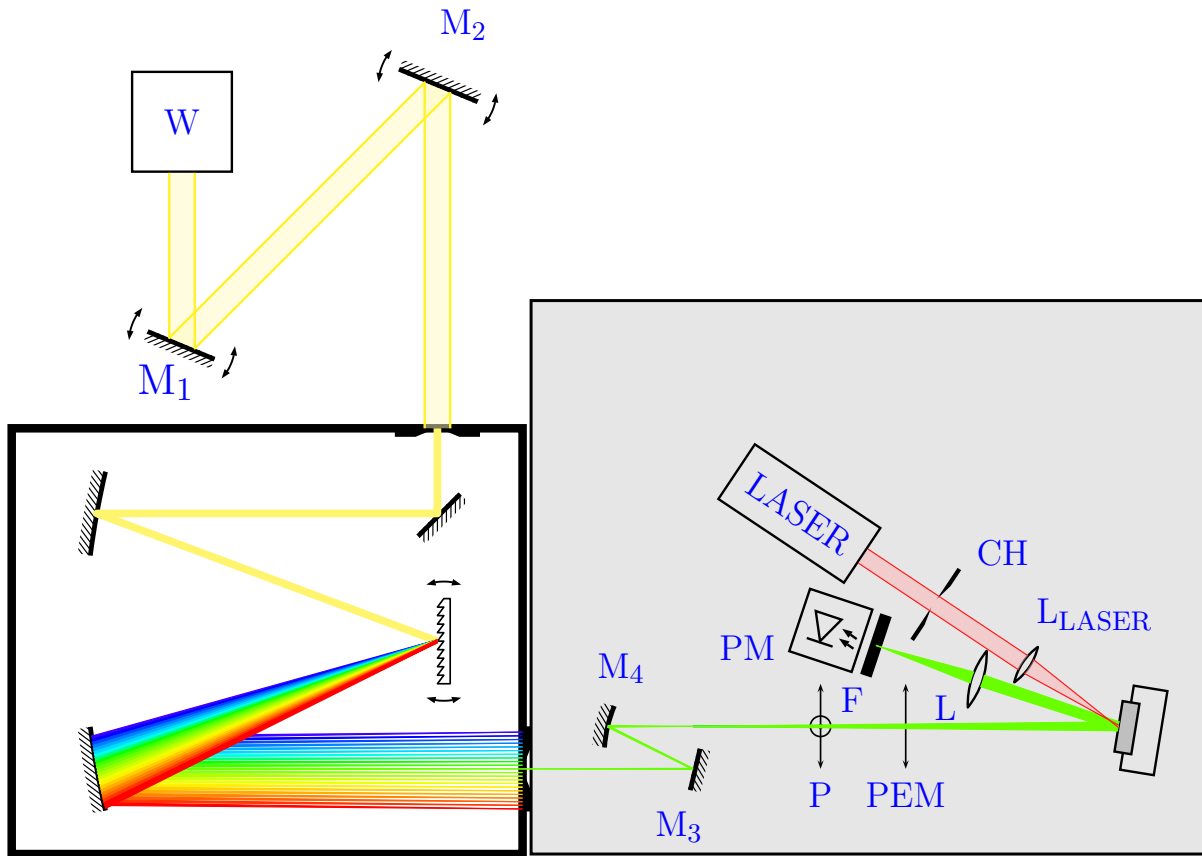


Figure 1.9: Photoreflectance setup used in these experiments, the setup implemented is commonly called dark configuration this due that photo-detector are exposed, then keeping closed to ambient light. W: tungsten lamp, M₁ to M₄ variable mirrors, P: polarizer, PEM: photoelastic modulator, L: focus lens, F: filter, PM: photomultiplier, L_{LASER}: focus lens for laser, CH: mechanical chopper.

The experimental setup to PR experiments implemented in this work, shown in Figure 1.9. The setup start with the probe light from a tungsten lamp, the beam is led by two silver mirrors to monochromator entrance slit, then the monochromatic beam passes through a polarizer and a photoelastic modulator finally affects on sample. The reflected light is focus to the PM with a focus lens. Modulation of the electric field in the sample is caused by photo-excited electron-hole pairs created by the pump source in our case is a red laser

that illuminates the same spot of the monochromatic beam and is chopped to a certain frequency, in this setup we use a mechanical chopper at 1KHz. It is important to mention that the reflected light in addition to being focused by a lens, is filtered before incide at PEM, this is important because the reflected laser light by the sample can modify the modulated R signal, do not forget that the PL signal is involved too.

Although the R signal is modulated by the chopper at 1KHz, after is measure by a lock-in amplifier due to the change in the R is very small about of 1×10^{-4} , in comparison with the PL signal, R change is less than PL as one million times. This is the reason by which any modulated spectroscopy commonly uses a lock-in amplifier. In our case, the setup is called Dark [35] setup because the PM is exposed to room light, therefore the system is keep closed. The Dark configuration has some advantages, one of these is, that the R changes are subtracted intrinsically therefore the use of the filter is enough to the dispersion of laser isn't a problem. We refer intrinsically to the R signal modulation. If the PL signal achieves to be detected, the system will perform subtraction as shown in Equation (1.6), if the PL signal mixes with the R in both cases this will cancel because it is constant, staying only the change in R.

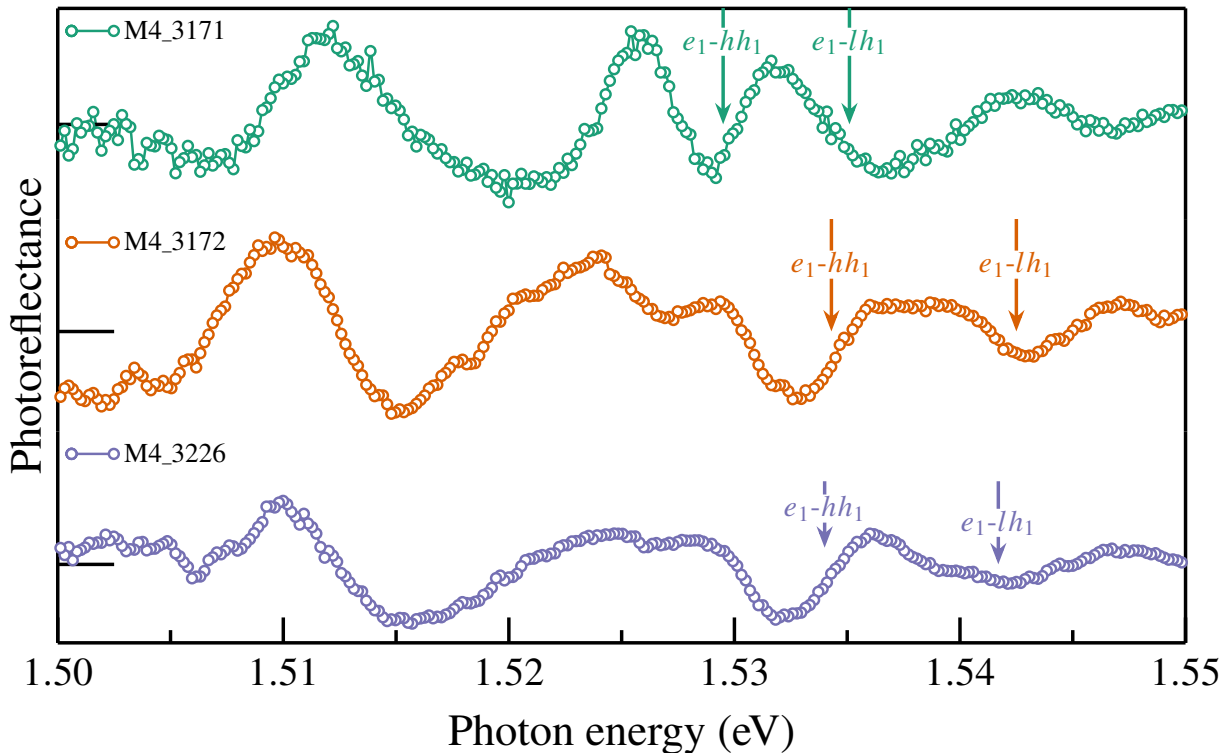


Figure 1.10: PR experiments to samples: M4_3171, M4_3172 and M4_3226 at 30K. Arrows point to calculated transitions for each sample, the used laser wavelength was the same, which in PL experiments and the power used in each of these was 5mW. Dashed line point the GaAs substrate.

The result of PR signals associated with band to band and quantum level transitions,

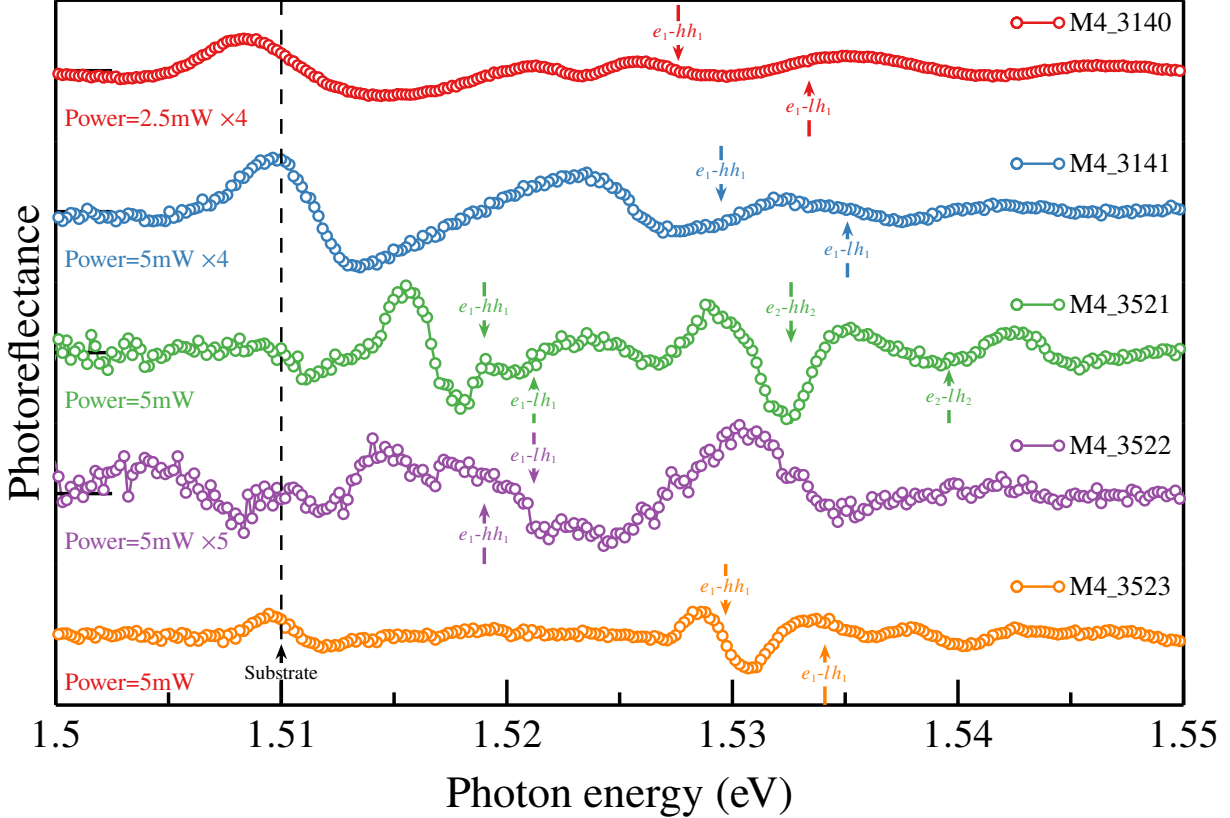


Figure 1.11: PR experiments to samples: M4_3140, M4_3141, M4_3521, M4_3522 and M4_3523 at 30K. Arrows point to calculated transitions for each sample, the used laser wavelength was the same, which in PL experiments and the previous PR experiments. Dashed line indicate the GaAs substrate, in these samples this transition is well located. The PR spectra of sample M4_3522 p-type doped (orange) is five times smaller than their correspond n-type, the sample M4_3521. The experiments in sample M4_3140 was performed at 2.5mW, then was multiply it by four in according to samples M4_3521 and M4_3523, in case of the sample M4_3141 even if, was performed at a power = 5mW the result was 5 times smaller than sample M4_3521. The discussion about of this is explained in the text.

in case of samples M4_43171, M4_43172 and M4_43226 the built-in electric field is low due to the structure n-i-n, this in principle is canceled or screen, this mean that the field create by carriers is opposite. The Figure 1.10 shows the result of PR experiments on samples mentioned above and are a bit informative. In fact, GaAs gap isn't visible in these samples, many mechanisms can affect the PR results in these. The first one and more representative undoubtedly is the low built-in field, if the structures are n-i-n the field expected is so low although the field can affect the interfaces and contribute but in general this is cancel by opposite photo-carrier directions. Frequently the PR is used tool to calculate or estimate intrinsic fields, this is possible in intermediate-field regimen, this known as Franz-Keldysh oscillations (FKOs) by electric field along z -direction [40]. So, the in PR spectra is observed oscillations and the period is determined by the field in the structure, where typically only about 3-4 FKO can be detected in the space charge region

of a doped sample. In this case for these samples and as will be explained later, the PR experiments are complex in context to determine all transitions that occur in them and the field is smaller, therefore does not are candidates to have FKOs.

The samples n-i-n type as shown in the Figure 1.10 the FKOs does not exist and this is clearly observable because these experiments does not have any oscillations, as before mentioned this behavior may be occurred because the directions of photocarriers generated are opposite, then the intrinsic field is canceled. Thus, the PR measured spectra are the result of modulation of intrinsic residual electric field or nonuniform fields effects [41]. In contrast, with the n-i-n type samples, the i-n type samples exposes clearly the direct transitions even associated to transitions with more energy (next levels energies), although the intrinsic field is not enough to generate FKOs.

In the Figure 1.11 can see the direct transitions numerically calculated for samples M4_3140, M4_3141, M4_3521, M4_3522 and M4_3523. The sample M4_3521 was taken as reference in terms of amplitude, in the sample M4_3140 was performed experiments as a function of power laser, being the power 2.5 mW the closest at 5mW, this is one of the reasons for that the result spectra was approx four times smaller than the sample M4_3521. The sample M4_3522 p-type, maybe can be five times smaller than their n-type analogous sample (M4_3521), but the line shape resultant does not have any response, i.e., in terms of amplitude is smaller, but the transitions aren't clarified or not resolved. This is one of our keys to final results because it has to do with carrier distribution and the nonexistence of the built-in electric field. For the sample M4_3141 the PR spectra is similar to the sample M4_3140, the difference between these structures is the barrier width, but in spectra the transitions are more resolved in the sample M4_3141.

From now on, we focus on the samples : M4_3140, M4_3521, M4_3522 and M4_3523, these samples are similar in structure, if shows experiments of the n-i-n type samples and the rest of i-n type samples is only to remark the importance of our results.

Even though in many works about the PR is normal to submit a line shape fit model to clarify the effects of modulated intrinsic fields around of critical points or transitions and as before mentioned this doesn't the interest of this work. Although, the study and models of line shape for modulated spectroscopy as the PR are essential in the experimental study of semiconductor physics [42, 43]. Nevertheless, in our experiments although the PR mechanism is observable in general around of the Gap (E_0) and direct transitions, the mechanism of modulation over the low intrinsic field, exhibit effects which is not frequently in the PR experiments, as it's shown in the following section.

1.2.2.1 Excitonic effects

THE CQWs structures are useful to study excitonic effects under external perturbations of an applied electric field. These structures are coupled by the thin barrier, then the electrons overlap over both wells, this behavior is very studied by the confinement effects and possibility to create devices based on electron properties. In this work, we focus on the samples which exhibit exciton effects that commonly are observed under external field apply in our case, without external fields or external perturbations and nor any structure modifies*. Starting with a comparison between ACQWs n- and p-type these are the M4_3521 and M4_3522 samples respectively, Figure 1.12(a) shows the PR of both samples(left), where the p-type sample is approx five times smaller than the n-type sample, therefore we can conclude that the mechanism of photo-carriers generated in these are different even if it has the same CQWs structure.

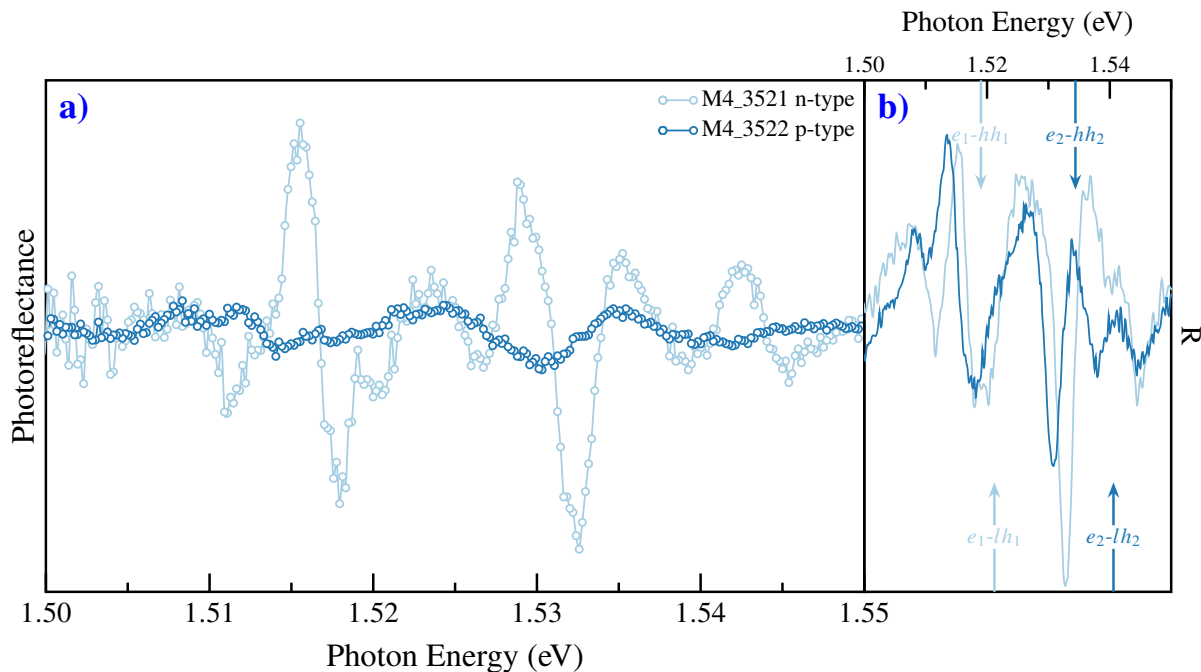


Figure 1.12: Comparison of : a) PR spectra of the 3521 (n-type) and 3522 (p-type) samples, the p-type sample is 5 times smaller than n-type sample. b) R spectra obtained at same time in each experiment, the arrows point to each direct transitions for two first confined energies. The line shape is practically the same in both spectra.

Also, the R spectra as shows the Figure 1.12(b) obtained synchronously at each experimental measured, this is the DC signal detected by photomultiplier and reading by the multimeter. These signals are practically the same, according to equation eq. (1.6) the change originated

*This refers to create strain by polish over the samples or mechanisms which generates strain, external perturbations also refers to temperature changes, applied currents, and others.

by the laser source doesn't enough, i.e., $\Delta R = R_{\text{off}} - R_{\text{on}}$ is smaller. In another way, the comparison of samples M4_3521 (ACQWs-2) and M4_3523 (SCQWs), shown in the figure Figure 1.13 exhibits the difference in amplitude at same power laser but around de E_0 is well resolved in both. In case of the SCQWs sample the direct transitions are well resolved, but in ACQWs-2 sample, could be present forbidden transitions, pointed at Figure 1.13 with same color of its correspond PR spectra. This behavior it has been observed previously [44] in MQWs structures even at 300K [45]. The nomenclature to allowed transitions (direct transitions) is: en-hhm for electron-heavy hole and en-lhm for electron-light hole, n index represent the n-th conduction subband and m-th valence subband. So, when $n=m$ its refer to direct transitions or allowed transitions, in ACQWs appear peaks related to transitions between first electron energy where electron wave function is predominantly in the wide well, but this wave function is overlapping to narrow well even if in minor percent, this mean that $n \neq m$ then the heavy- and light-holes confined at narrow well can create e1-hh2, e1-lh2 transitions, or the electrons in second confined energy that predominantly are at narrow well but, they can penetrate (tunneling) to the another well (wide well) as seen in Figure 1.13 can generate another forbidden transitions. It's important to mentioned that this behavior is presented at low-field regime, therefore can't associate this to modulation of the built-in electric field, this being discussed since some years ago [45, 46], even though can this associated, with the behavior which have the electron, heavy- and light-holes in CQWs structures, with a specific barrier width and the height of the potential barriers (or depth of wells) [11, 47]. The electron and holes tunneling depends on those parameters and, in our case, the barriers potential depends on Al percent in the alloy $\text{Al}_x\text{Ga}_{1-x}\text{As}$, therefore $x = 0.15$ then the barriers they are not so tall, and the coupling barrier width is very thin ($< 2 \text{ nm}$).

These structures, become an interesting platform to study the phenomenology and behavior of confined electrons, heavy- and light-holes, and their respective interactions. Another interesting phenomenon, which we could observe, was the triions (\mathbf{X}^+ or \mathbf{X}^-) formation through the PR experiments. When were carried out the set of PR experiments over the samples i-n type, occurred a peculiar event while we performed and established the correct measure parameters, to be specific while we determined the laser power. This doesn't mean that our experiments are wrong, as a matter of fact, this peculiar event made us test the experimental setup several times and carried out experiments as a function of laser power. This event started with the M4_3140 (ACQWs-1) sample, this sample has a well with a slightly wide width and because of that the wave function overlapping in major percent than the others samples, by this reason is reasonable or expected, that the triions formation it's more likely as explain later. While they were being carried out, the PR experiments in ACQWs-1 sample, at higher power laser allowed by our device, in fact, this was trouble, because the laser power doesn't stable, so it was decided to turn on the laser previously before performing each experiment, this was around of eight hours before to start experiments. After detecting the problem with the laser power, it was started

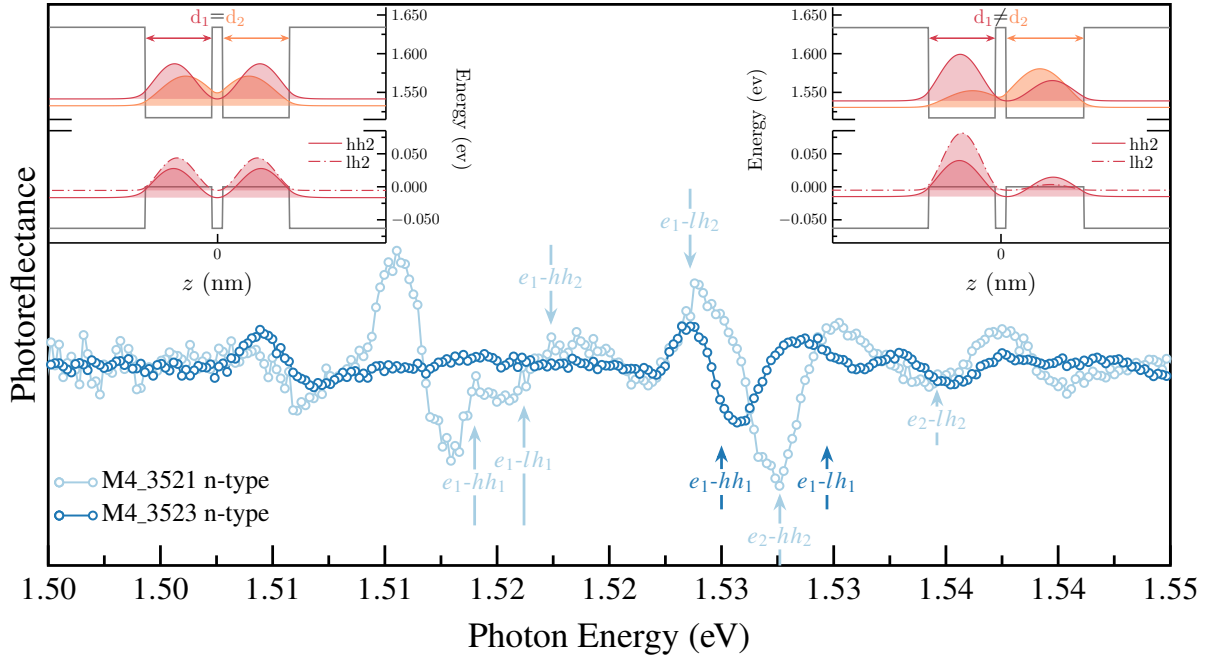


Figure 1.13: The PR comparison between samples M4_3521 (ACQWs-2) and M4_3523 (SCQWs), the electron wave function are plotted for each sample where, the SCQWs sample at top left and at top right to ACQWs sample. The top arrows pointed to forbidden transitions in ASQWs-1 sample, while the bottom arrows pointed to the direct transitions in both samples.

the PR experiments at higher laser power, the results were peculiar due to appearing a higher peak with respect to direct transitions, in fact, the direct transitions didn't was observable. These experiments were realized several times and the behavior was kept, then we decided to increase the spectral resolution to try to understand the nature of this peak, previously all experiments were carried out with the monochromator slits at 1500μ this to enhance the light collected by PM. The Figure 1.14 shows the evolution of these experiments at $P=50\text{mW}$ as a function of the slits aperture, it's clearly that doesn't about of experimental contraption or another external thing which can contribute or being the cause of this behavior.

From these results it decided all experiments with these apertures of slits, although we try to enhance the spectra resolutions at $750\mu\text{m}$ was they got the best results. In the Figure 1.15 shows the evolution of the PR spectra as a function of laser power, starting with 1mW of power and finished with 50mW . Remember previously mentioned that the laser power is unstable and this trouble it didn't allow performing the experiments increases power in one way more uniform, this is the reason that the experiments were carried out with powers at 1mW , 3mW , 8mW , 30mW , and 50mW . The spectra with power less than 8mW are relatively similar, therefore, after that power it can see a change in peak width and that peak tends to shift at less energy.

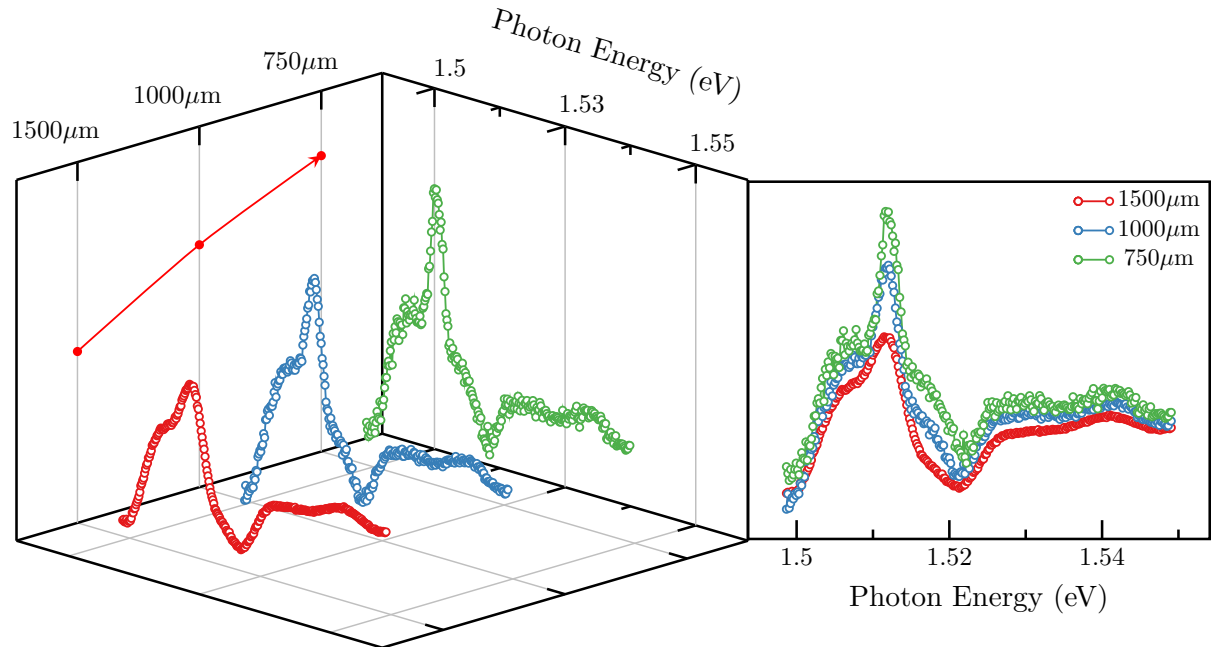


Figure 1.14: PR spectra of the ACQWs-1 sample designed as a function of slits aperture, where it can see the increase of peak resolution as decrease the aperture of slits.

Now, we establish the physical background of that rare behavior in the PR experiments. In semiconductors, the electron-hole pairs are the reason for many special phenomena and are commonly called the hydrogen atoms in semiconductors. But to understand the nature of excitons and their consequent behaviors, it needs to start with a specific platform to keep or extend their life and interactions. As above-mentioned, the life of the excitons in QWs is extended for several reasons, of which; well width and low temperatures enhance the binding energy [48, 49]. When the light interacts with these structures, the electron-hole pair associated with the absorption of a photon with enough energy results in an exciton (general explanation), but if inside the structure the electron density is great [50], the excitons and all possible interactions which can occur as exciton-exciton, exciton-hole (X^-), exciton-electron(X^+), electron-electron, even, LO-phonon-exciton interaction. All of this presents in a modification of the line shape resultant, in terms of the PL experiments it's possible to observe unexpected transitions as a slight modification in the line shape. In spite of the physics involved in this mechanism is very complex, the hard work in this theme has generated valuable results.

Since the 50s Lampert [51] suggested the existence of charged excitons also called *trions* in semiconductors and after almost 40 years it's proved experimentally [50, 52], and as expected the trions X^+ or X^- they were observed in QWs. The electron concentration has a role important in trion formation, for this reason, they usually modulated n- or p-type doping in the QWs structures. Also, the external perturbations as the electric* or

*In this case the trions formation is due a relative position of the Fermi level when the low electric

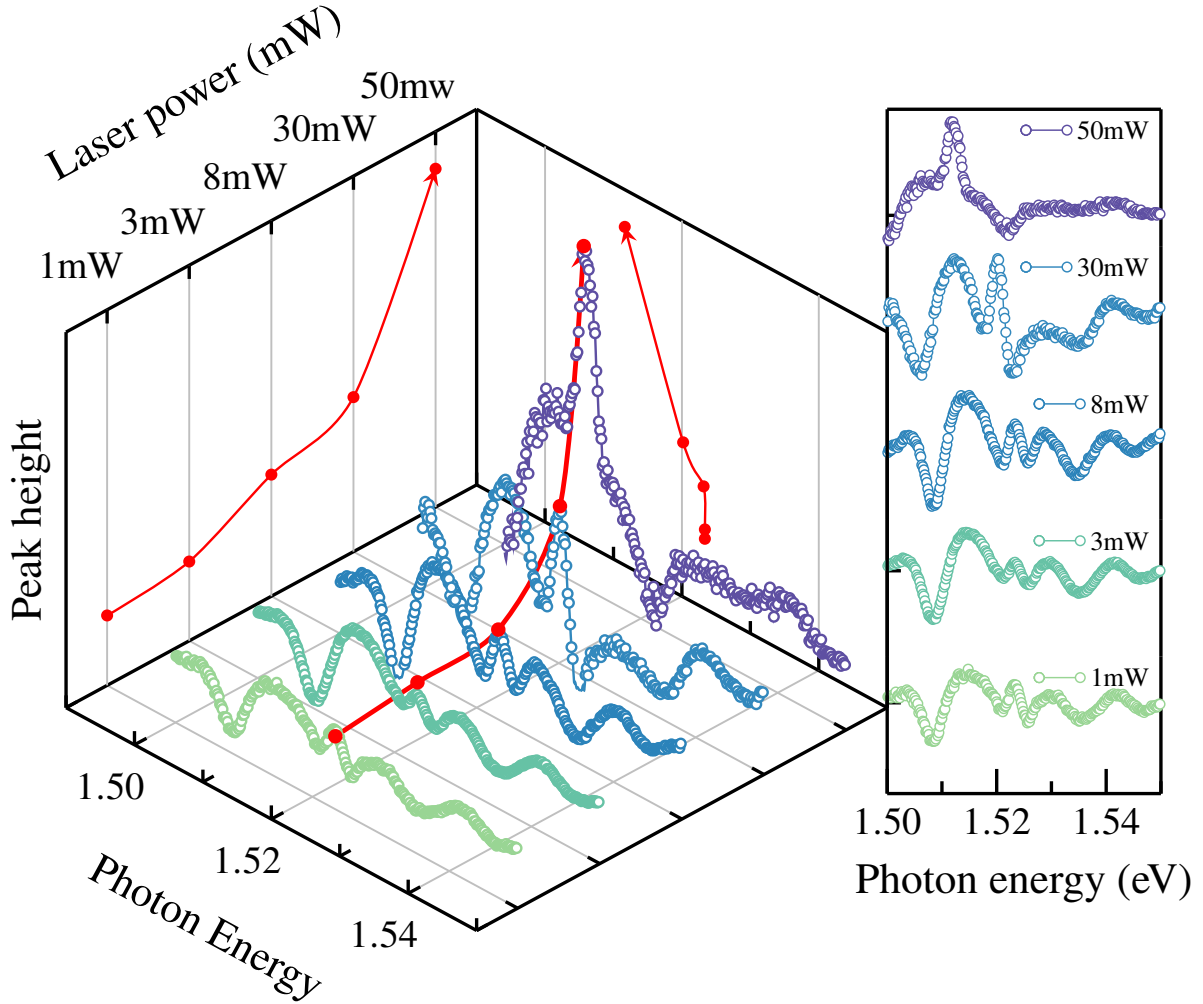


Figure 1.15: The peak tends to height as increase the laser power, which also is very observable as a redshift.

magnetic fields commonly used to enhance the trions transitions, in the magnetic field case, the trions involved acquiring a triplet state nature, so the Zemman splitting is expected, therefore the transitions are well resolved. At zero field, the ground state of trion is a singlet [53], this is, two electrons with opposite spin, these electrons are bound with a hole as shows the scheme in Figure 1.16(a).

In our case, the trions formation is due to photo-excited carriers induced by the laser source, if we suppose that the doped layer is the absolute answer of this, the other samples as SCQWS-1 and ACQWS-2 would have similar results in their PR spectra when it increases laser power, but this is not observed, in fact, in these cases the line shape kept

field is applied, in fact, the mechanism involves indirect transitions and is easy that the indirect exciton interact with elctrones or holes [17].

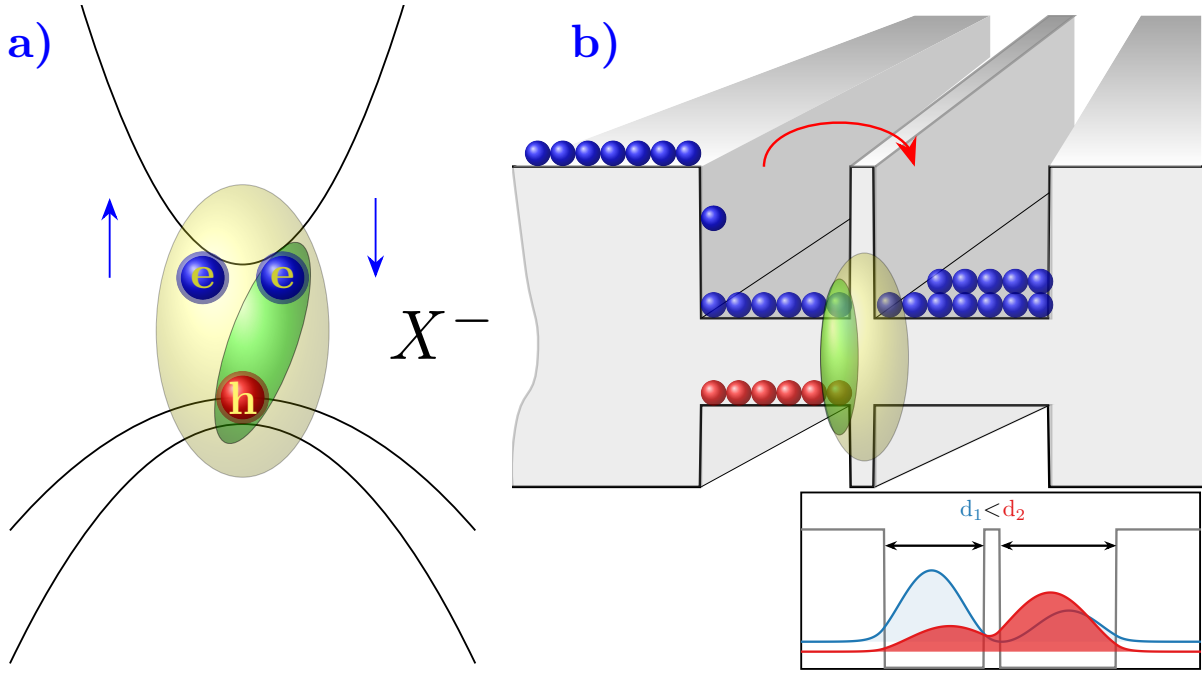


Figure 1.16: Trions formation scheme in terms of band structure (a) in this case, the exciton is bound to an electron in the conduction band leading to a three-body system knew as negative trion \mathbf{X}^- . On the other hand, in (b) it presents the possible formation of \mathbf{X}^- due to a slight width of one in the CQWS, consequently, the narrow well transfers electrons through tunneling to a wide well, if it's calculated the wave functions of this structure, the wave functions have the characteristic of to be distributed asymmetrically as in the case of the applied electric field along z [11, 12].

but noisily, then if we adjudicate the trion formation to photo-excited carriers, which is the cause that enables trions in the ACQWs-2 sample?. The answer is a hypothesis that needs extra experiments but is part of the future objectives of this work. The electron and holes (hh , lh) wave functions in samples slightly asymmetric in wells widths, i.e., one of the wells is slightly width than the other, these wave functions have similar behavior as the case when de electric filed is applied. This behavior enhances the electron tunneling from the narrow well to the other well (wide well) as shows in Figure 1.16(b), if all-important samples contain the doped layer with the same n-type concentration if we suppose that this layer modifies the Fermi level thus generating a small electron gas (2DEG), its possible think that this electron gas has a function of electron reservoir [54, 55]. Then the photo-carriers generates by the laser source step up carriers dynamics, doing that the narrow well is yielding continuously electrons to wide well through tunneling and, these electrons are recombining with the excitons confined in the plane of the narrow well, therefore results in a three-body system $\mathbf{X}^- = (e, e, h)$ or $\mathbf{X}^+ = (e, h, h)$. As it's known, the trion is a charged exciton where the sign depends on its formation, in the case of $\mathbf{X}^- = (e, e, h)$ their transition is under the first transition of X_{hh} , and their energy evolution tends to redshift as can see in Figure 1.15. Therefore in our case, which

was also has been reported [50, 54–57], the shift evolution correspond to an \mathbf{X}^- trion, however still missing more experiments to strengthen this hypothesis. On the other hand, what happens if the 2DEG doesn't consider? It is very important to emphasize this argument because the objective of this work is to demonstrate that CQWS structures especially ACQWs shows effects of symmetry breaking doesn't see in structures without external perturbation(application of: electric or magnetic field, strain, etc.) or intentional modification (growing of interfaces that unbalance the QWs region, differences in the potential of the barriers), by this reason is importantly empathize that regardless of exist a 2DEG whichever is their electron density and the built-in electric field which can this generate, as a matter of fact, that field doesn't represent the cause of the phenomena presented in this work, more later this is discussed with more detail. On the other hand, is relatively easy to corroborate that the presence of the electric field on those samples can be regarded as despise, what is the reason to asseverate this if the PR has a principal characteristic the built-in field modulation? As before mentioned the non-existence of the FKOs is a point to assert the field regime is low, moreover, in comparison with the n-i-n-type samples, also remain in this regime notwithstanding of be designed to reduce the built-in field. However, it's can be estimated by means of Schrödiner-Poisson, so as to, the equation ?? it's coupled Poisson equation [58, 59]

$$\left(\frac{d}{dz} \varepsilon(z) \frac{d}{dz} \right) V_p(z) = \rho(z) \quad (1.7)$$

$$\left(\frac{d}{dz} \varepsilon(z) \frac{d}{dz} \right) V_p(z) = e \left[n_D(z) - \sum_i n_i^s |\psi_i(z)|^2 \right] \quad (1.8)$$

With the objective of present the behavior and the causes of the high doping in the $\text{Al}_x\text{Ga}_{1-x}\text{As}$ layer, we implement a simple code, starting off our numerical codes and helping us with already implemented codes as Aestimo [7], we calculated numerically Schrodinger-Poisson equation. It is important to mention which solution is self-consistent, therefore the code is implemented with all parameters to divergence avoid, in our case is due to high doping and this is too large.

For this reason, it is inevitable that the codes don't converge, although it can be considered a factor damping to speed convergence [60]. We consider the damping factor, and we decided to calculate a structure as GaAs/n-type doped $\text{Al}_x\text{Ga}_{1-x}\text{As}$ / $\text{Al}_x\text{Ga}_{1-x}\text{As}$, where the width of lateral layers is fixed and the width of the doped layer varies from 15nm to 300 nm with the same n-type doped $6 \times 10^{18} \text{ cm}^{-3}$. In general, the self-consistent Schrodinger-Poisson equation, is a process that starts with the calculation of the confined energies in the potential profile defined as $V(z)$, in this profile are included each parameter of the material that makes up the heterojunction as the doping quantity in each layer if this is doped. After, as shown in Equation (1.8), is evaluating the space charge with their respective charged donors and their concentration n_D , n_i^s is the electron sheet density of the confined levels and corresponding wavefunctions $\psi_i(z)$. To calculates the electron density in each level i frequently is applied Fermi-Dirac statistics [61–63].

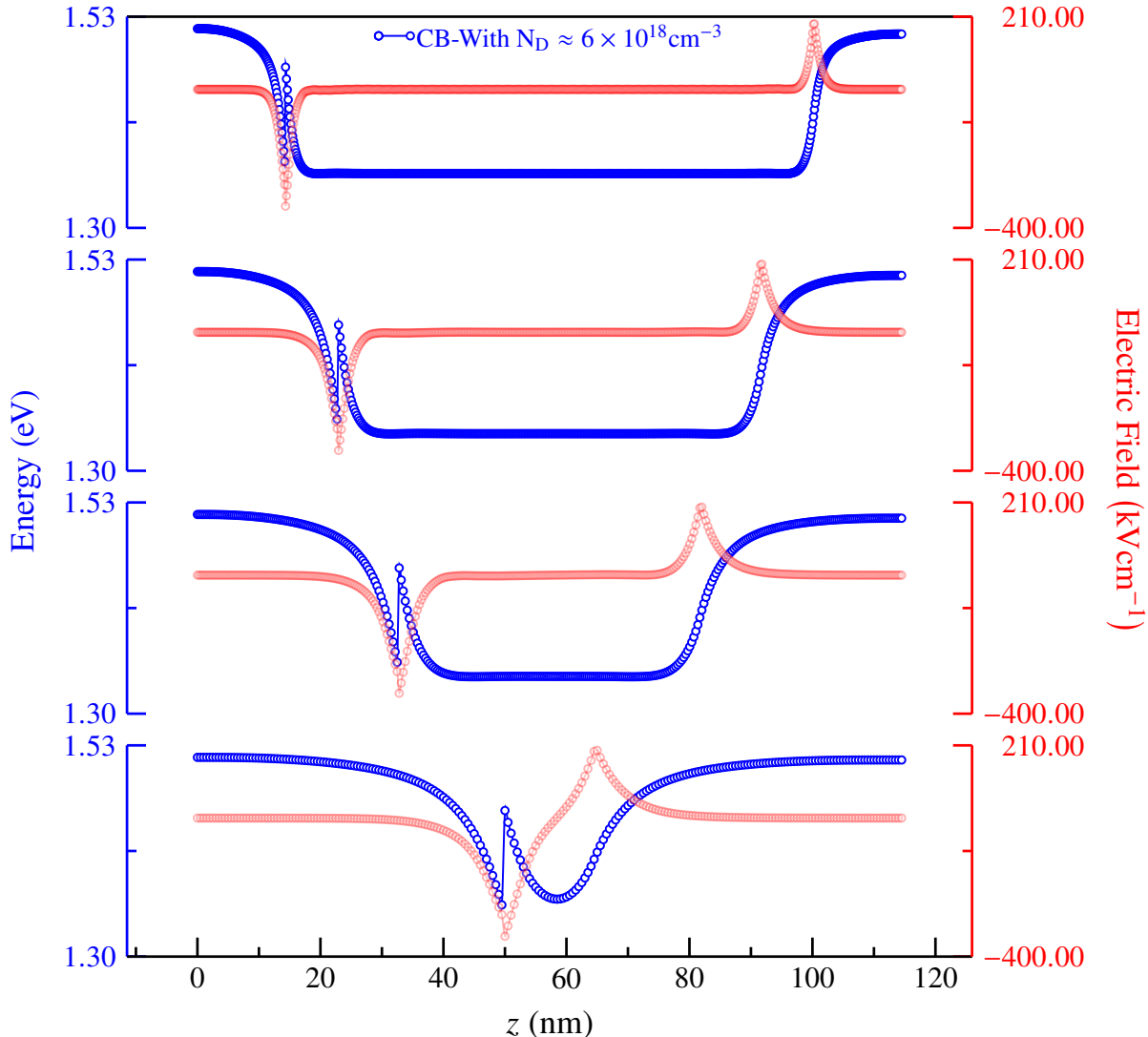


Figure 1.17: Results to self-consistently Schrodinger-Poisson equation, in order down to top the n-type layer Al_{0.15}Ga_{0.85}As doped ($6 \times 10^{18} \text{ cm}^{-3}$) is increasing in width from 15nm, 75nm, 150nm to 300nm. The goal of this is to calculate in a general way the effects of the doped layer, specifically due to the electric field induced by this. The strength of the field is expressed in kVcm units, although this magnitude si great, we assume that doesn't significantly, latter we explained this.

This charge distribution in the structure gives rise to space charge effects, resulting in an additional electrostatic potential V_p which causes conduction band bending [58, 64]. The total potential V is the result of $V = V_0 + V_p$, where the V_0 is the original potential profile, so, this is the iterative part of calculations, in our case, we established the difference between $e_{1\text{new}} - e_{1\text{old}} < 1 \times 10^{-5}$ as convergence factor. Previously mentioned the damping factor is defined for fast convergence, in our case α_{damp} is about 1×10^{-3} . The results are shown in Figure 1.17 to a structure : GaAs/Al_{0.15}Ga_{0.85}As(n-type $6 \times 10^{18} \text{ cm}^{-3}$)/Al_{0.15}Ga_{0.85}As with four different widths (15nm, 75nm, 150nm, and 300nm) for the layer doped.

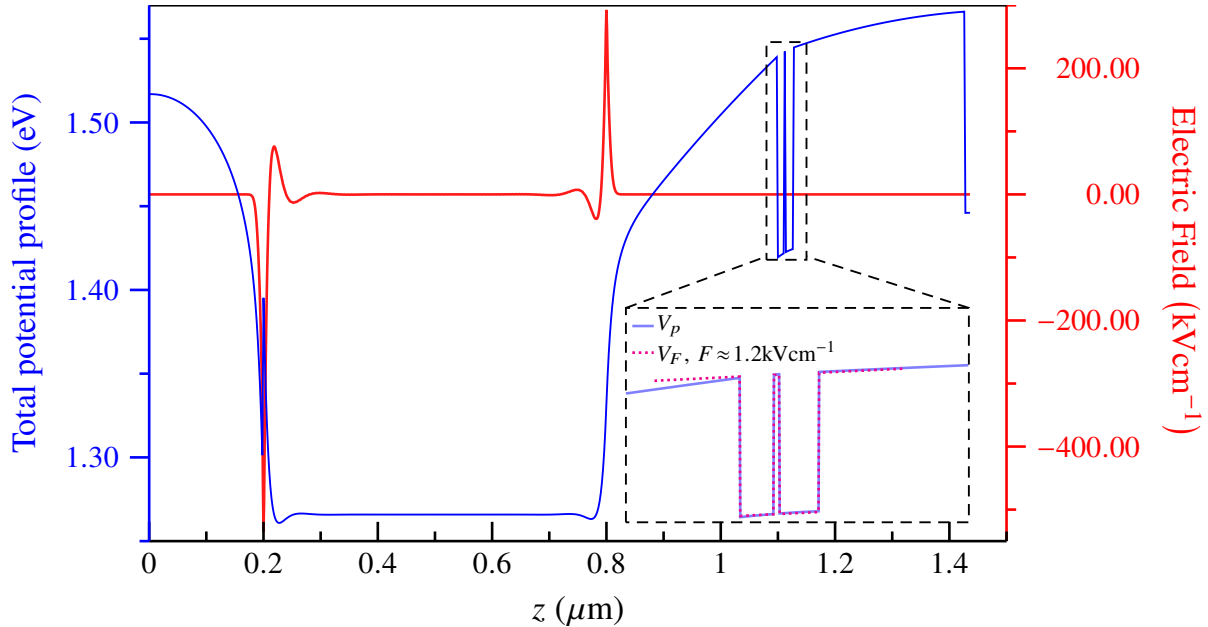


Figure 1.18: Band conduction profile $V(z)$ calculated by numerical solution of self-consistent Schrödinger-Poisson equation. The calculations were performed considering the width of the doped n-type 6×10^{18} layer with 600nm. The zoom inset shows the comparison between total potential calculated (blue) and when applied field $F \approx 1.2\text{kVcm}^{-1}$ (dotted magenta), where at around of CQWs zone are similar.

In the next chapter, we expose the RAS experiments and their significance in the wonderful results of this work, following, is important to define and explain the role of the doping layer that as can see may be generated a significant intrinsic field which in contrast with the RAS results and our model the built-in electric field doesn't significatively important in the symmetry breaking ($D_2 \rightarrow C_{2v}$). Therefore, we calculate the possible conduction band bending due to the built-in electric field as can see in Figure 1.18.

We have taken into account a total structure width with an n-type doped layer, we remember that the high doping and large width can cause the calculations doesn't converge by this we implemented a damping factor to accelerate the convergence, also we calculated a potential profile considering an external electric field applied around of $F \approx 1.2\text{kVcm}^{-1}$. The results show that practically the total V_p and electric field (line-shape and magnitude) are kept as shown in Figure 1.17, if we compare the potential profiles V_p and V_F as see in Figure 1.18, it can observe that practically the band bending which is generated by electric field so much as by doped layer, as an external field applied are very similar if the external potential is around of $F \approx 1.2\text{kVcm}^{-1}$. This means that, if exists an electric field but is comparable with surface field [65], hence is a small field. Therefore, we can say that the effects of the trions are associated with the asymmetry of the QWs as before mentioned.

1.2.2.2 The PR summary

In conclusion, the PR remains a powerful tool for experimental solid-state physics, especially in semiconductors study the facility to implement it, and the great information which gives as about fundamental transitions that in comparison with other spectroscopy is still better. Along with the experimental work, we could notice that the PR has the capability of detect behaviors which doesn't common in this spectroscopy as trions measured, and although this work is still in progress, the satisfaction to propound a novel source to study of an excitonic behavior as the trions, through easy spectroscopy without external perturbations. On the other side, the AQCWs has a large potential to study quantum phenomena, especially the interactions and process due to the exciton confined, in this case, something so simple as the relative widths in the CQWs generates a surprising behavior.

1.2.3 Reflectance Anisotropy Spectroscopy (RAS)

THE RAS is the experimental tool that completes the set in this work, without the intention of replicates the physical background and interpretations about RAS, we focus on specific terms to detail our great results. This spectroscopy, is a powerful tool in the studying of semiconductors physics, being characterized as default anisotropy study tool. This experimental technique, was developed by Aspnes [34, 66, 67] to measure *surface-induced* optical anisotropy in cubic semiconductors, although this can be applied around of near-band-edge [68]. So, to our purposes, RAS is an excellent experimental tool to study optical anisotropies in CQWs structures. In our case both RAS and PR setup is the same with their exceptions, in the PR case is necessary to add the laser to modulated spectroscopy while in the RAS the modulation it's realized by the PEM, which changes the polarization state. As schemes in Figure 1.19, the monochromatic light first times through over polarizer prism and the PEM to finally being focused onto the sample with spot size of 5.00mm diameter. The light reflected by the sample is collected and detected by the multialkali photomultiplier tube (before discussed in Section 1.1 and shows in Table 1.2). A detailed description of the RAS technique can be found elsewhere [69]. As shows in Figure 1.19, the RAS signal is proportional to:

$$\frac{\Delta R}{R} = 2 \frac{R_{[110]} - R_{[1\bar{1}0]}}{R_{[110]} + R_{[1\bar{1}0]}} \quad (1.9)$$

where denotes the orientations $[110]$ and $[1\bar{1}0]$ over crystalline directions(see Figure 1.1). In our experiments the RAS signal is around of 10^{-4} . As well's known if the RAS signal it's detected, the structure exhibits an optical anisotropy for in-plane light propagation [70]. The experiments, as the PR case, were it performed at 30K.

In accordance with ??, the anisotropy into these structures entails into interesting physical phenomena, overall about of optical properties. This IOA it's due to the hole mixing, as a long as the structures being under symmetry reduction, in this case from $D_{2d} \rightarrow C_{2v}$. If we measured RAS over SCQWs, it's expected that this doesn't exhibit an IOA or failing that this being smaller due to abrupt interfaces are non-ideal.

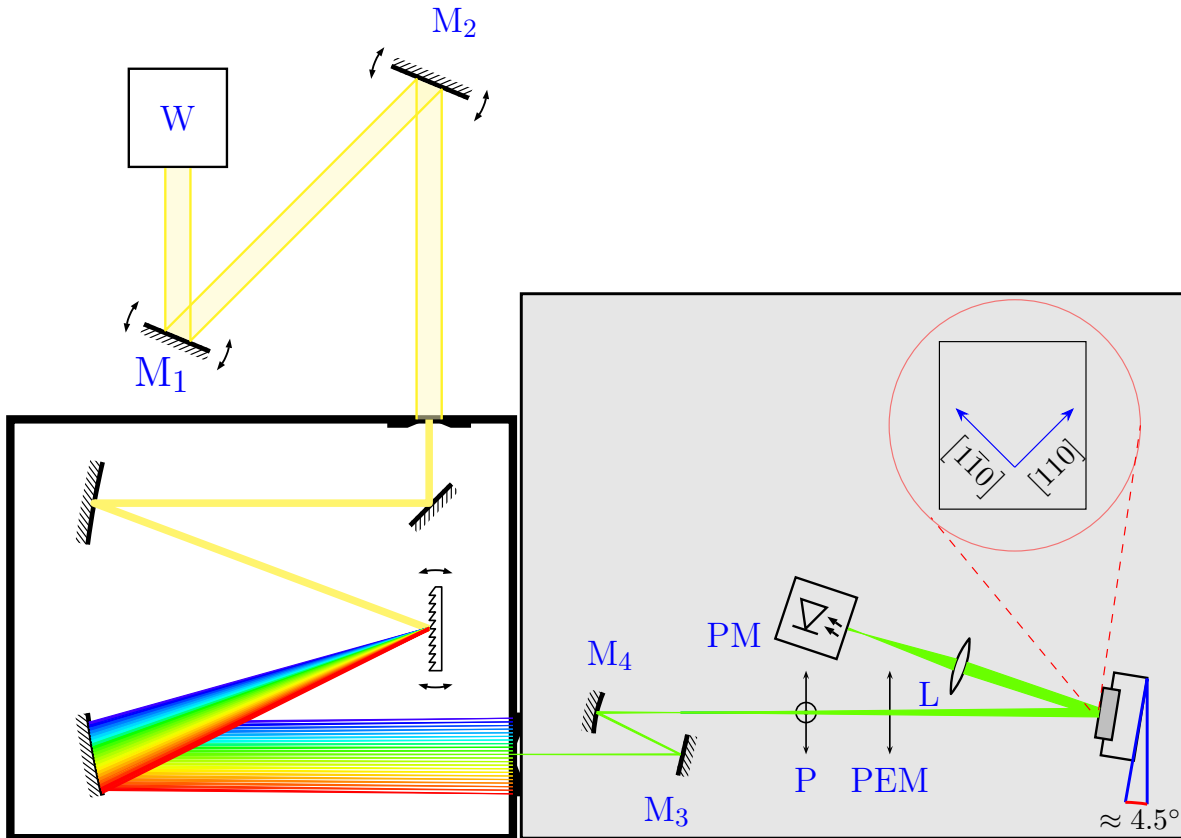


Figure 1.19: RAS setup implemented in this work, as before explained in the PR setup, this is a dark configuration this due that photo-detector are exposed, then keeping closed to ambient light. The optical array is the same as the PR, with the difference which the role of polarization and PEM. This figure also schemes the incidence angle which is about of 4.5° and the directions of linear polarization.

The first part of experiments were carried out over the samples: M4_3171, M4_3172 and M4_3226, we remember that these samples are the type n-i-n, this means that they consist in more growth layers, therefore it's expected that the RAS signal being smaller. The Figure 1.20 shows the results to these samples, in top to bottom order, in left side plots the RAS while in right side it's plotted the R spectra. The R spectra plotted to each sample is the average of all experiments performed, this means which in each RAS experiment, the glsR was simultaneously measured, then to each sample it's taking the average. In order to discuss the result of that samples, we can observe that in general therm these samples gets a smaller signal of RAS, although in R it does not happen, the direct transitions can

being locate in accordance with the numerical results as shows with arrows.

Although these three samples consists in more several growth layers, it's possible to measure an in-plane anisotropy were in samples: M4_3171 and M4_3226 the signal amplitude it's relatively same in contrast with the sample M4_3171.

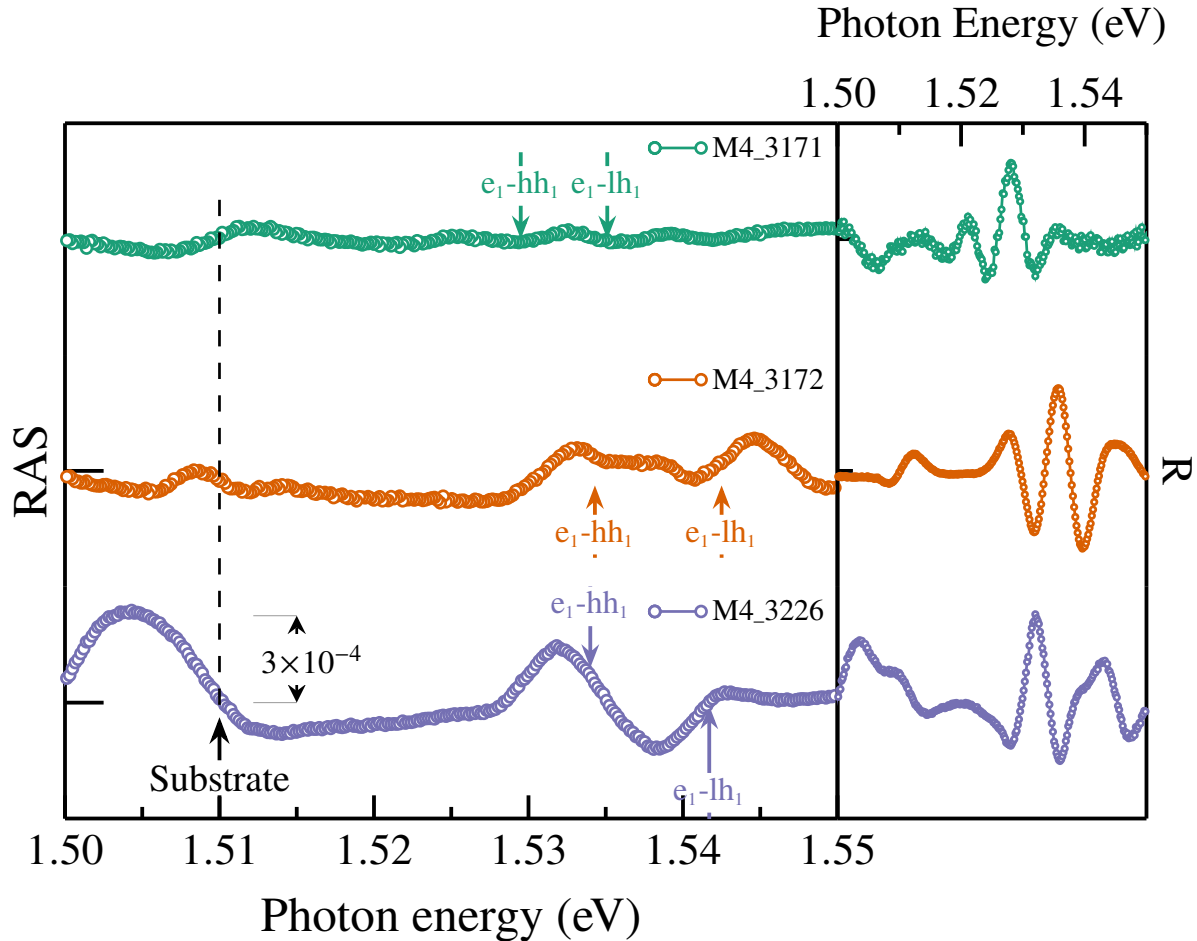


Figure 1.20: Experimental results from samples: M4_3171, M4_3172 and M4_3226, from top to bottom respectively. In left, shows the RAS result where with a dashed line it's denote the substrate transition, in each sample denotes the direct transitions with arrows. The right side, show the plots of R spectra, which is the average result of all experiments carried in each correspond sample.

The first RAS results even they are an asymmetric CQWs structures, the RAS spectra it's higher in the samples with AlAs barrier (M4_3172 and M4_3226), then the potential barrier is higher than in the sample M4_3171, but the width of these barriers is small, therefore we have a case with samples they consist; in high coupled barrier and thinner. In the other sample, where the RAS spectra is smaller (M4_3171), the coupled barrier is small in potential in comparison with the other samples, but is more wide.

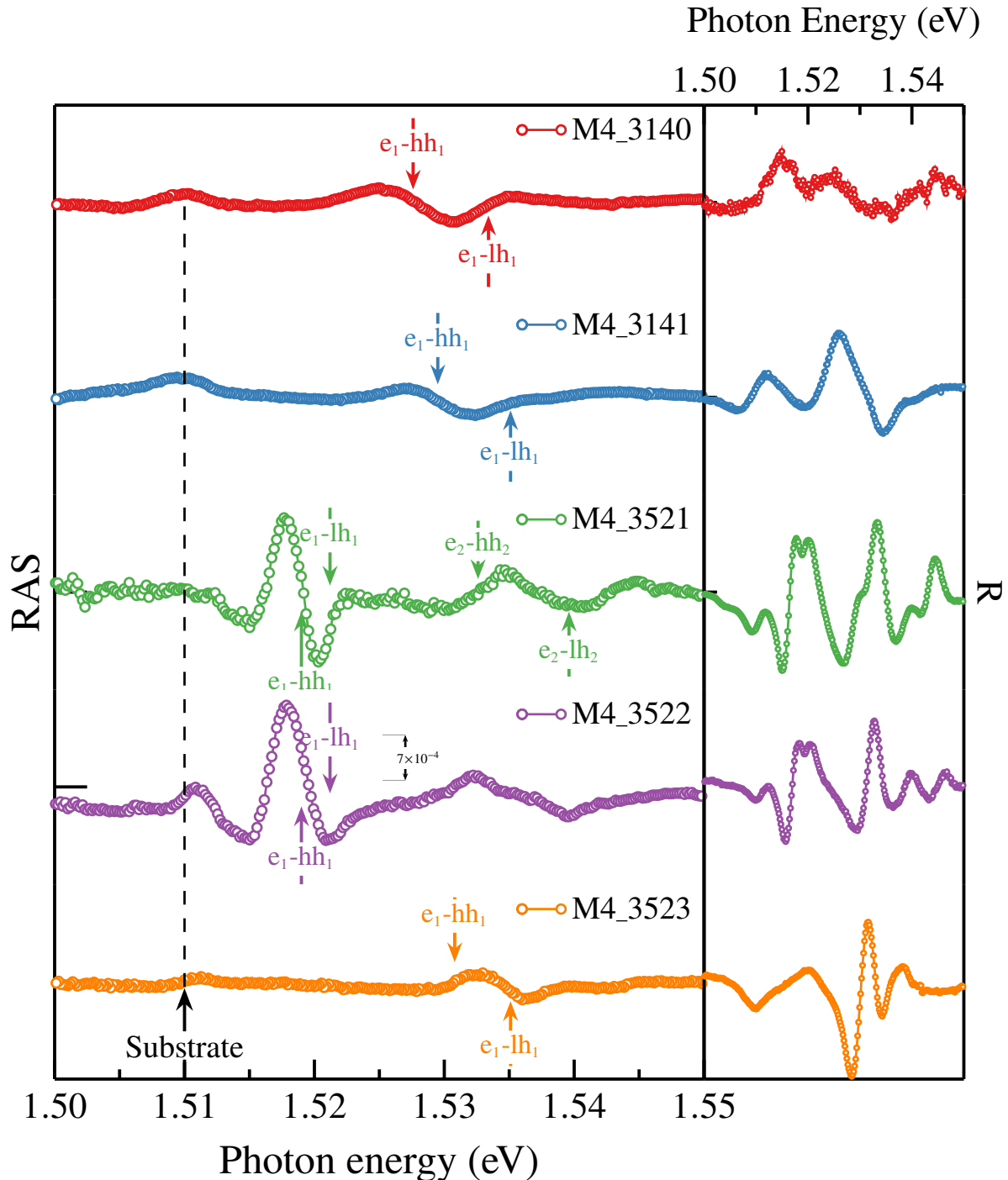


Figure 1.21: Experimental results from samples: M4_3140, M4_3141, M4_3521, M4_3522 and M4_3523, from top to bottom respectively. In left, shows the RAS result where with a dashed line it's denote the substrate transition, in each sample remarks the direct transitions with arrows. The right side, show the plots of the R spectra, which is the average result of all experiments carried in each correspond sample. Also, it's denote the RAS magnitude proportional to 7×10^{-4} , which in contrast with SCQWs samples the signal is smaller. The direct transitions it's locate by two peaks with opposite concavity where can see that the larger one transition is $e_1\text{-}hh_1$ and smaller one associated with the $e_1\text{-}lh_1$.

Although, it was expected that the spectra relatively same in these three samples, the coupled barrier plays an important role this due to the tunneling process, wells it returns a RAS spectra more definite (better line-shape) than the sample with less tunneling, this means, the coupled barrier is wide. Then, the sample M4_3171 is approx three times smaller. These samples are relatively common with barrier exception, in sample M4_3226 that better has RAS response posses a coupled barrier with a width of 0.424 nm, while the second with a better RAS response is the sample M4_3172 which has a barrier width of 0.565 nm.

In the next set of samples: M4_3140, M4_3141, M4_3521, M4_3522 and M4_3523, as is explained in Section 1.1, consists in samples with coupled barrier of $\text{Al}_{0.15}\text{Ga}_{0.9}\text{As}$, where the difference in this set samples, is one of these samples (M4_43141) has a coupled barrier twice wider than the other samples, and the relative width of the wells.

The Figure 1.21 shows the results of RAS experiments carried out on these samples. These results are interesting in comparison with the before set, the most notorious is the evolution of RAS signal in the more asymmetric structures, in these structures the peaks associated with direct transitions are seen more clearly, being those with an opposite concavity. In these peaks the larger one it's the heavy-hole (down concavity) while the smaller one it's the light-hole transition (up concavity). It's totally evident that the samples M4_3521 and M4_3522 (also called as ACQWs-1 and ACQWs-2) exhibits great RAS response, then, in accordance with the model anisotropy has a major hole mixing. Also, the R spectra is well resolve in both samples, with a peculiarity in the transitions concavities, which in both, is up concavity.

1.2.3.1 RAS strength discussion and the physical model justification

To enter into discussion, its purpose is to focus on the three samples before mentioned, aiming to expose the principal objective of this work, which is denoted the RAS strength in ACQWs as importance in the optical properties and excitonic effects in these structures. The Figure 1.22 exposes the evolution of RAS strength, in this plot it is indisputable that the signal increases, because the comparison between the three samples where it's starting with a symmetric structure, then with a lightly asymmetric structure and finally with a very asymmetric structure, the RAS signal associated with each transition have opposite concavities and redshift as the structure is more asymmetric.

Due to the fact that the wave-function probability density of sample SCQWs is distributed symmetrically along the QW structure, the IOA strength is expected to be similar to that obtained for a single QW. In fact, a RAS signal of the order of magnitude of 0.1×10^{-3} has been reported for an 8 nm single QW [71], which has the same order of magnitude as the spectra of Figure 1.23(c). This IOA is attributed to the inequivalent AlGaAs/GaAs interfaces along the SCQWs structure. It's important every clear the role of tunneling in the coupled wells, the difficulty to get a model to explain this structures doesn't it the

same as the single QW structure.

As pointed out before (??), the strength of the IOA signal is produced by an intermixing of the heavy- and light-hole states in the valence band that is proportional to $\langle \psi_{hhn} | \mathcal{H} | \psi_{lhn} \rangle$ according to ???. For the lowest heavy- and light-hole levels ($n = 1$), there is an estimated separation in energy of around $\Delta E_1 = 2.0, 4.1$, and 4.4 meV for samples ACQWs-2 (ACQWs-3), ACQWs-1, and SCQWs, respectively. The mixing $\langle \psi_{hhn} | \mathcal{H} | \psi_{lhn} \rangle$ can be estimated by considering that the transitions are direct (n is the same for the valence and conduction band) and then the overlapping terms in ?? must be approximately the same for each sample. For transitions $n = 1$ it can be seen in Figure 1.22 that amplifier ratios of the spectra between ACQWs-2 and ACQWs-1 with respect to SCQWs are 1.5 and 3.7, respectively. Thus from ?? we estimate ratios of $\langle \psi_{hh1} | \mathcal{H}_{ACQWs-1} | \psi_{lh1} \rangle / \langle \psi_{hh1} | \mathcal{H}_{SCQWs} | \psi_{lh1} \rangle \sim 1.4$ for sample ACQWs-1 and $\langle \psi_{hh1} | \mathcal{H}_{ACQWs-2} | \psi_{lh1} \rangle / \langle \psi_{hh1} | \mathcal{H}_{SCQWs} | \psi_{lh1} \rangle \sim 1.7$ for sample ACQWs-2.

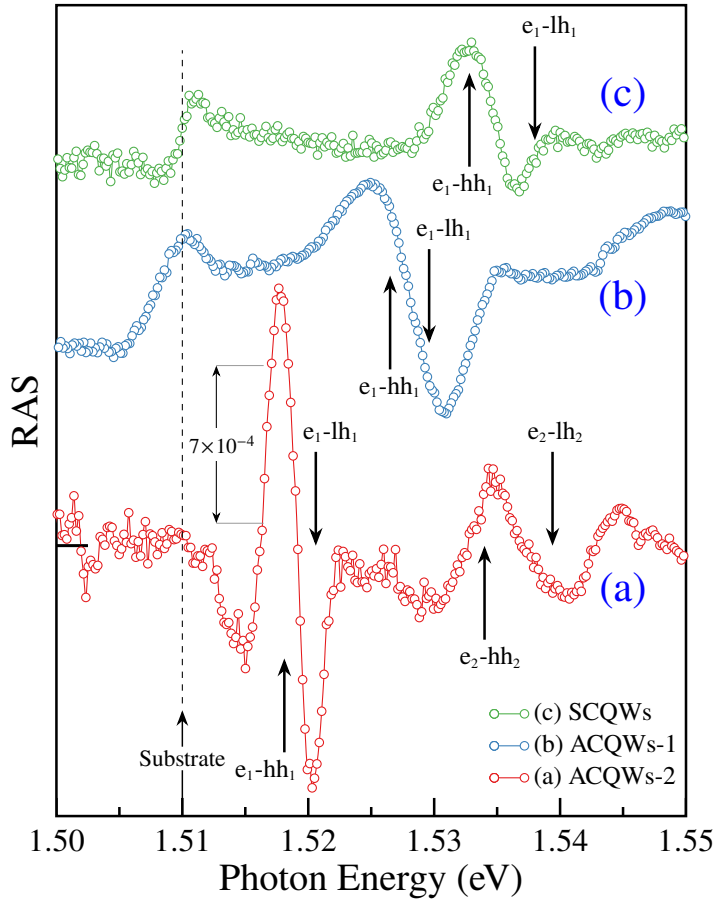


Figure 1.22: RAS spectra for the (a), (b), asymmetric and (c) symmetric CQWs. The dashed vertical line indicates the expected energy of the excitonic transition of the GaAs substrate. Above this energy, the optical transitions come from the DQWs. The inset shows the PL spectra measured for each sample. Two peaks can be identified in each spectrum, a larger one associated with the transition $e1-hh1$ and a much smaller one associated with the $e1-lh1$ [for spectrum (b) this peak is observed as a shoulder]. The energies obtained from the PL spectra are indicated by the arrows in the RAS spectra. Note that the structures associated with $e1-hh1$ and $e1-lh1$ increase their strength when the DWQs become more asymmetric. The RAS spectra were measured at 30 K.

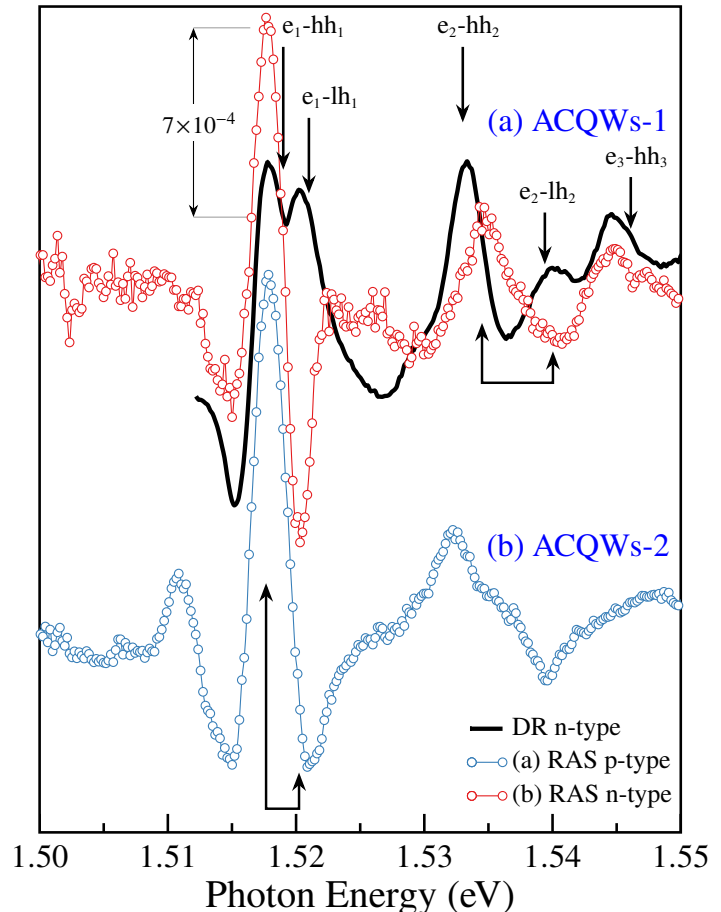
In accordance with our estimation based on the anisotropy model, the Table 1.5 contains the energies considered. If well, the large IOA in general, it's attributed to interfaces in our case the reason is due to non-equivalence due to the width asymmetric into coupled QWs, this originates a mixing of hh-lh states and therefore these it coupled strongest as

Sample	e1-hh1	e1-lh1	ΔE_e (meV)	ΔE_{hh} (meV)	ΔE_{lh} (meV)	ΔE_n (meV)
SCQWs	(N)1.5328 (E)1.5297	(N)1.5380 (E)1.5341	8.9	0.9	6.9	$\Delta E_1 = 4.4$ $\Delta E_2 = 10.5$
ACQWs-1	(N)1.5265 (E)1.5273	(N)1.5296 (E)1.5314	8.4	1.3	6.4	$\Delta E_1 = 4.1$ $\Delta E_2 = 9.2$
ACQWs-2	(N)1.5181 (E)1.5190	(N)1.5206 (E)1.5210	11.8	3.4	7.5	$\Delta E_1 = 2.0$ $\Delta E_2 = 6.4$

Table 1.5: Comparative of experimental (E) and numerical calculations (N) of first level transition energies (in eV). δE_e , δE_{hh} and δE_{lh} corresponds to the difference between electrons, heavy- light holes states, respectively. ΔE_n is the numerical calculation of energy splitting for transitions 1 and 2 ($n = 1, 2$).

the states close in energy [72]. The Table 1.5 and ?? confirms this, in the ACQWs-2 this energy between hh1 and lh1 states are close, in counterpart with the SCQWs this energy is large.

Figure 1.24: Reflection anisotropy (RAS, (a), (b)) and differential reflection (DR, solid line) spectra for ACCQWs-2 and ACQWs-3, grown on an AlGaAs n-type and p-type layer respectively. Note that while for the heavy hole transitions ($e_1\text{-}hh_1$ and $e_2\text{-}hh_2$) in the RAS and DR spectra have the same concavity, for light holes transitions ($e_1\text{-}lh_1$ and $e_2\text{-}lh_2$) the concavities are opposite and DR spectra shows the highest level transitions. The bottom arrows point to the experimental transitions for the two first levels, whereas the top arrows show the calculated energies to three energy levels. The RAS and DR spectra were measured at 30K.



In order to elucidate the physical origin of the RAS in the ACQWs, we compare in Figure 1.24 the RAS and the DR spectra of the ACQWs-2. DR spectra is obtained by the numerical subtraction of the reflection (R) spectra recorded at 30K and 300K followed by the normalization to the 300K spectrum. The subtraction highlights the excitonic features, which are very weak (and energy shifted) at 300K. The comparison between RAS and DR spectra allows us to contrast the contribution of the heavy and light holes transitions. Around 1.5175 eV, the DR spectrum shows two peaks corresponding to e1-hh1 and e1-lh1 transitions. Note that in the RAS spectrum, the structure associated to e1-hh1 transition has the same concavity as the corresponding for the DR spectrum, while the e1-lh1 transition has the opposite concavity. This is an indication of the transfer of oscillator strength between the levels due to the intermixing of heavy- and light- holes, thus supporting our anisotropy model. The same behavior applies for the e2-hh2 and e2-lh2 transitions at around 1.5375 eV. Transition e2-hh3 is also indicated and it has the same concavity for RAS and DR spectra, as in the case of the e1-hh1 and e2-hh2 transitions. The arrows at the bottom of Figure 1.24 indicate the energy of the states en-hhn and en-lhn (for n = 1 and 2) obtained from the maximum and minimum of the RAS spectrum. From the numerical calculation results summarized in Table 1.5, the energy splitting between transitions en-hhn and en-lhn are $\Delta E_1 = 2.0$ meV and $\Delta E_2 = 6.4$ meV. In accordance with ??, the IOA amplitude is proportional to $1/\Delta E_n$. Considering the same valued for the overlapping and the mixing $\langle \psi_{hhn} | \mathcal{H} | \psi_{lhn} \rangle$ we estimate an amplitude ratio of 3.25 between these transitions. This value is close to the value of 3.9 obtained by the RAS spectrum of Figure 1.24 supporting our interpretation.

Finally, we discuss the possible contribution to the RAS amplitude by an built-in electric field accross the CQWs both symmetric and asymmetric. To study this contribution, we have compared the RAS spectra of asymmetric samples ACQWs-2 and ACQWs-3. The difference between them is the doping of the AlGaAs layer (see Table 1.1). While for ACQWs-2 it is n-type, for ACQWs-3 it is p-type. Assuming that the built-in electric field originates from charge transfer between surface states and the AlGaAs doped layer (n or p), this field is expected to have opposite signs for samples ACQWs-2 and ACQWs-3 . Thus, the linear contribution of the electric field to the RAS should be reversed in sign for such samples. Figure 1.26 shows the comparison between the RAS spectra of samples ACQWs-2 and ACQWs-3, this with aim to demonstrate that in the case of existed a field the sign is opposite. The experiment, it was designed to measure both samples in a sequence way along the same preferential direction, in this case we choose the direction of pits [1̄10] [13], if existed a field we expected a opposite RAS signal, but this doesn't occur, the sign in signal it was conserved in both samples. The Figure 1.26 shows the results of this experiment, in top left and right it's placed the images of both samples of the pits orientation, this to corroborate that the direction of measured. As can be seen (Figure 1.24), RAS spectra are equivalent in shape and have the same sign, thus indicating that the contribution of the electric field to the RAS signal is very small.

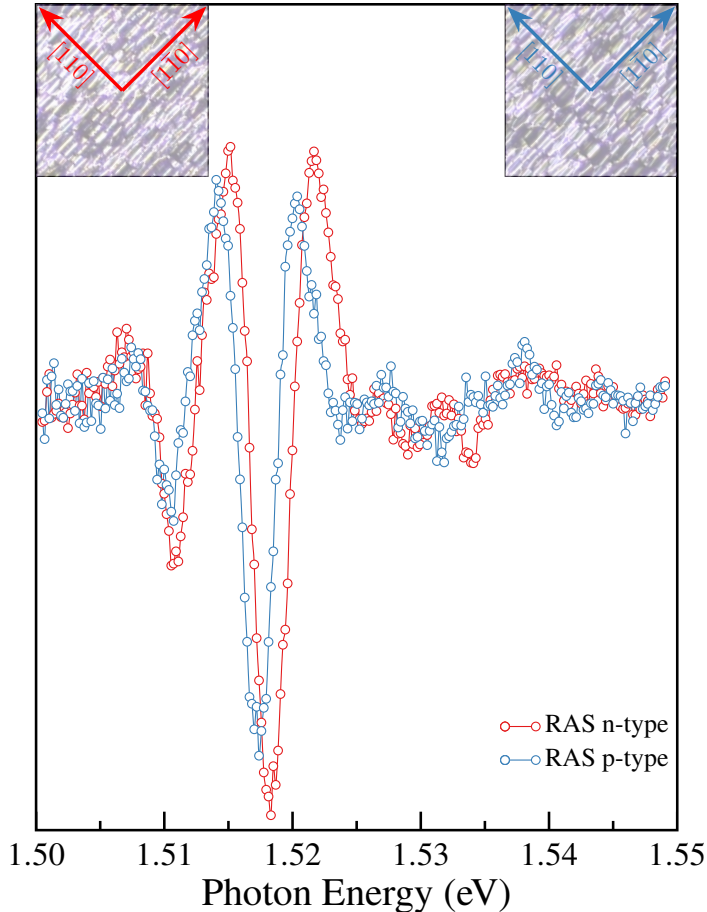


Figure 1.26: RAS experiment designed to demonstrate the non-existence of built-in electric field through sequential measured along the preferential direction, in this case, it was chosen along the pits $[1\bar{1}0]$ [13]. The signal result in both samples practically is the same, the sign is conserving. At top left and right located the images taken with a microscope of back substrate which shows the pit reveals along of $[1\bar{1}0]$ direction.

It's natural to suppose that the built-in electric field contributes to increase of the RAS signal, and although we estimate that this field is small, it is still important to discuss it and show different ways to affirm that the built-in field isn't the reason of the IOA. We conclude, thus, that the dominant contribution to RAS spectra is the asymmetry of the CQWs system.

1.2.3.2 The RAS summary

In conclusion, the RAS proves experimentally that the IOA increases as a degree of asymmetry in CQWs structures. This behavior is attributed to the reduction of the symmetry of the electronic states in the CQWs with QWs of different thicknesses. The nature of the transitions was identified by using PL spectroscopy and numerical calculations. We believe that the results presented in this work are important and will be useful in understanding the evolution of the optical transition induced by the breakdown of translation symmetry in asymmetric CQWS.

BIBLIOGRAPHY

- [1] O. Ruiz-Cigarrillo and G. Martinez-Cepeda, “Coupled quantum wells codes,” 2018. [Online]. Available: <https://github.com/lflmgroup/cqws-codes.git> (Cited on page IV.)
- [2] J. Bezanson, A. Edelman, S. Karpinski, and V. B. Shah, “Julia: A fresh approach to numerical computing,” *SIAM Review*, vol. 59, no. 1, pp. 65–98, 2017. [Online]. Available: <https://pubs.siam.org/doi/10.1137/141000671> (Cited on page IV.)
- [3] G. Martinez-Cepeda and O. Ruiz-Cigarrillo, “**k · p** julia package,” 2022. [Online]. Available: <https://github.com/lflmgroup/kp-lflm-group.git> (Cited on page IV.)
- [4] A. H. Larsen, J. J. Mortensen, J. Blomqvist, I. E. Castelli, R. Christensen, M. Dułak, J. Friis, M. N. Groves, B. Hammer, C. Hargus, E. D. Hermes, P. C. Jennings, P. B. Jensen, J. Kermode, J. R. Kitchin, E. L. Kolsbjerger, J. Kubal, K. Kaasbjerger, S. Lysgaard, J. B. Maronsson, T. Maxson, T. Olsen, L. Pastewka, A. Peterson, C. Rostgaard, J. Schiøtz, O. Schütt, M. Strange, K. S. Thygesen, T. Vegge, L. Vilhelmsen, M. Walter, Z. Zeng, and K. W. Jacobsen, “The atomic simulation environment—a python library for working with atoms,” *Journal of Physics: Condensed Matter*, vol. 29, no. 27, p. 273002, 2017. [Online]. Available: <http://stacks.iop.org/0953-8984/29/i=27/a=273002> (Cited on page IV.)
- [5] A. Togo and I. Tanaka, “**Spglib**: a software library for crystal symmetry search,” 2018. (Cited on page IV.)
- [6] D. Alonso-Álvarez, T. Wilson, P. Pearce, M. Führer, D. Farrell, and N. Ekins-Daukes, “Solcore: a multi-scale, python-based library for modelling solar cells and semiconductor materials,” *Journal of Computational Electronics*, vol. 17, no. 3, pp. 1099–1123, 2018. (Cited on pages IV and 11.)
- [7] H. Hebal, Z. Koziol, S. Lisesivdin, and R. Steed, “General-purpose open-source 1d self-consistent schrödinger-poisson solver: Aestimo 1d,” *Computational Materials Science*, vol. 186, p. 110015, 2021. [Online]. Available: <https://www.sciencedirect.com/science/article/pii/S0927025620305061> (Cited on pages IV and 27.)
- [8] K. Momma and F. Izumi, “it VESTA3 for three-dimensional visualization of crystal, volumetric and morphology data,” *Journal of Applied Crystallography*, vol. 44, no. 6, pp. 1272–1276, Dec 2011. [Online]. Available: <https://doi.org/10.1107/S0021889811038970> (Cited on page IV.)
- [9] T. Tantau, “Pgf/tikz,” 2007. [Online]. Available: <https://github.com/pgf-tikz/pgf.git> (Cited on page IV.)

- [10] C. Bersch, “pst-optexp, drawing optical experimental setups,” 2022. [Online]. Available: <https://github.com/cbersch/pst-optexp> (Cited on page IV.)
- [11] K. Sivalertporn, “Effect of barrier width on the exciton states in coupled quantum wells in an applied electric field,” *Physics Letters A*, vol. 380, no. 22, pp. 1990–1994, 2016. [Online]. Available: <https://www.sciencedirect.com/science/article/pii/S0375960116300664> (Cited on pages VII, 22, and 26.)
- [12] N. Debbar, S. Hong, J. Singh, P. Bhattacharya, and R. Sahai, “Coupled gaas/algaas quantum-well electroabsorption modulators for low-electric-field optical modulation,” *Journal of Applied Physics*, vol. 65, no. 1, pp. 383–385, 1989. [Online]. Available: <https://doi.org/10.1063/1.342554> (Cited on pages VII and 26.)
- [13] J. L. Weyher and J. J. Kelly, *Defect-Selective Etching of Semiconductors*. Berlin, Heidelberg: Springer Berlin Heidelberg, 2010, pp. 1453–1476. [Online]. Available: https://doi.org/10.1007/978-3-540-74761-1_43 (Cited on pages IX, 37, and 38.)
- [14] N. V. Tkachenko, *Optical spectroscopy: methods and instrumentations*. Elsevier, 2006. (Cited on pages X, 6, and 7.)
- [15] J. W. Orton and T. Foxon, *Molecular beam epitaxy: a short history*. Oxford University Press, USA, 2015. (Cited on page 2.)
- [16] M. Grundmann, *Physics of semiconductors*. Springer, 2010, vol. 11. (Cited on page 2.)
- [17] M. Yuan, A. Hernández-Mínguez, K. Biermann, and P. V. Santos, “Tunneling blockade and single-photon emission in gaas double quantum wells,” *Phys. Rev. B*, vol. 98, p. 155311, Oct 2018. (Cited on pages 5 and 25.)
- [18] J. Weiner and F. Nunes, *Light-matter interaction: physics and engineering at the nanoscale*. Oxford University Press, 2017. (Cited on page 5.)
- [19] A. Einstein, “Über die von der molekularkinetischen theorie der wärme geforderte bewegung von in ruhenden flüssigkeiten suspendierten teilchen,” *Annalen der Physik*, vol. 322, no. 8, pp. 549–560, 1905. [Online]. Available: <https://onlinelibrary.wiley.com/doi/abs/10.1002/andp.19053220806> (Cited on page 6.)
- [20] C. A. Bravo-Velazques, “Sistema de fotoluminiscencia para caracterización de pozos cuánticos acoplados,” 2 2020, bachelor Thesis to obtain Engineering Physicist degree. (Cited on page 8.)
- [21] S. Chuang, *Physics of Optoelectronic Devices*, ser. Wiley Series in Pure and Applied Optics. Wiley, 1995. [Online]. Available: <https://books.google.com.mx/books?id=ect6QgAACAAJ> (Cited on page 10.)

- [22] J. Jimenez and J. W. Tomm, *Spectroscopic Analysis of optoelectronic semiconductors*. Springer, 2016, vol. 202. (Cited on pages 10 and 11.)
- [23] W. Lu and Y. Fu, *Spectroscopy of Semiconductors*. Springer International Publishing, 2018. [Online]. Available: <https://doi.org/10.1007/978-3-319-94953-6> (Cited on page 11.)
- [24] D. W. Ball, *The basics of spectroscopy*. Spie Press, 2001, vol. 49. (Cited on page 11.)
- [25] W. Demtr̄der, *Electrodynamics and Optics*. Springer Nature, 2019. (Cited on page 11.)
- [26] J. Solé, L. Bausa, and D. Jaque, *An introduction to the optical spectroscopy of inorganic solids*. John Wiley & Sons, 2005. (Cited on page 11.)
- [27] H. Khmissi, L. Sfaxi, L. Bouzaïene, F. Saidi, H. Maaref, and C. Bru-Chevallier, “Effect of carriers transfer behavior on the optical properties of inas quantum dots embedded in algaas/gaas heterojunction,” *Journal of Applied Physics*, vol. 107, no. 7, p. 074307, 2010. [Online]. Available: <https://doi.org/10.1063/1.3371356> (Cited on page 14.)
- [28] J. Kundrotas, A. Čerškus, S. Ašmontas, G. Valušis, B. Sherliker, M. P. Halsall, M. J. Steer, E. Johannessen, and P. Harrison, “Excitonic and impurity-related optical transitions in be δ -doped GaAs/AlAs multiple quantum wells: Fractional-dimensional space approach,” *Phys. Rev. B*, vol. 72, p. 235322, Dec 2005. [Online]. Available: <https://link.aps.org/doi/10.1103/PhysRevB.72.235322> (Cited on page 14.)
- [29] J. Singh, K. Bajaj, and S. Chaudhuri, “Theory of photoluminescence line shape due to interfacial quality in quantum well structures,” *Applied physics letters*, vol. 44, no. 8, pp. 805–807, 1984. (Cited on page 15.)
- [30] F.-Y. Juang, J. Singh, P. K. Bhattacharya, K. Bajema, and R. Merlin, “Field-dependent linewidths and photoluminescence energies in gaas/algaas multiquantum well modulators,” *Applied physics letters*, vol. 48, no. 19, pp. 1246–1248, 1986. (Cited on page 15.)
- [31] J. Maluenda and P. M. Frijlink, “Abrupt transitions in composition and doping profile in GaAs/Ga_{1-x}Al_xAs heterostructures by atmospheric pressure movpe,” *Journal of Vacuum Science & Technology B: Microelectronics Processing and Phenomena*, vol. 1, no. 2, pp. 334–337, 1983. [Online]. Available: <https://avs.scitation.org/doi/abs/10.1116/1.582552> (Cited on page 15.)
- [32] B. V. Shanabrook, O. J. Glembotki, and W. T. Beard, “Photoreflectance modulation mechanisms in gaas-al_xga_{1-x}as multiple quantum wells,” *Phys. Rev. B*, vol. 35, pp. 2540–2543, Feb 1987. [Online]. Available: <https://link.aps.org/doi/10.1103/PhysRevB.35.2540> (Cited on page 16.)

- [33] B. O. Seraphin and D. E. Aspnes, “Electric field effects in optical and first-derivative modulation spectroscopy,” *Phys. Rev. B*, vol. 6, pp. 3158–3160, Oct 1972. [Online]. Available: <https://link.aps.org/doi/10.1103/PhysRevB.6.3158> (Cited on page 16.)
- [34] D. Aspnes and D. Sell, “Surface field effects in reflectance and first-derivative modulation spectra,” *Solid State Communications*, vol. 13, no. 5, pp. 519–522, 1973. (Cited on pages 16 and 30.)
- [35] J. Misiewicz, G. Sek, and P. Sitarek, “Photoreflectance spectroscopy applied to semiconductors and semiconductor heterostructures.” *Optica Applicata*, vol. 29, no. 3, pp. 327–363, 1999. (Cited on pages 16, 17, and 18.)
- [36] M. Sydor, J. Angelo, J. J. Wilson, W. C. Mitchel, and M. Y. Yen, “Photoreflectance from gaas and gaas/gaas interfaces,” *Phys. Rev. B*, vol. 40, pp. 8473–8484, Oct 1989. [Online]. Available: <https://link.aps.org/doi/10.1103/PhysRevB.40.8473> (Cited on page 16.)
- [37] W. M. Theis, G. D. Sanders, C. E. Leak, K. K. Bajaj, and H. Morkoc, “Excitonic transitions in gaas/ga_xal_{1-x}as quantum wells observed by photoreflectance spectroscopy: Comparison with a first-principles theory,” *Phys. Rev. B*, vol. 37, pp. 3042–3051, Feb 1988. [Online]. Available: <https://link.aps.org/doi/10.1103/PhysRevB.37.3042> (Cited on page 16.)
- [38] W. M. Theis, G. D. Sanders, K. R. Evans, L. L. Liou, C. E. Leak, K. K. Bajaj, C. E. Stutz, R. L. Jones, and Y.-C. Chang, “Extrinsic contributions to photoreflectance of al_xga_{1-x}as/gaas quantum wells: An investigation of the “donor-related” feature,” *Phys. Rev. B*, vol. 39, pp. 11 038–11 043, May 1989. [Online]. Available: <https://link.aps.org/doi/10.1103/PhysRevB.39.11038> (Cited on page 16.)
- [39] I. Gontijo, Y. Tang, R. De La Rue, C. Sotomayor Torres, J. Roberts, and J. Marsh, “Photoreflectance and photoluminescence of partially intermixed gaas/algaas double quantum wells,” *Journal of applied physics*, vol. 76, no. 9, pp. 5434–5438, 1994. (Cited on page 16.)
- [40] H. Shen and M. Dutta, “Franz–keldysh oscillations in modulation spectroscopy,” *Journal of Applied Physics*, vol. 78, no. 4, pp. 2151–2176, 1995. [Online]. Available: <https://doi.org/10.1063/1.360131> (Cited on page 19.)
- [41] R. Del Sole and D. E. Aspnes, “Effect of surface and nonuniform fields in electroreflectance: Application to ge,” *Phys. Rev. B*, vol. 17, pp. 3310–3317, Apr 1978. [Online]. Available: <https://link.aps.org/doi/10.1103/PhysRevB.17.3310> (Cited on page 20.)
- [42] M. Cardona, “Modulation spectroscopy,” *Solid State Phys.*, vol. 11, 1969. (Cited on page 20.)

- [43] B. O. Seraphin and N. Bottka, “Band-structure analysis from electro-reflectance studies,” *Phys. Rev.*, vol. 145, pp. 628–636, May 1966. [Online]. Available: <https://link.aps.org/doi/10.1103/PhysRev.145.628> (Cited on page 20.)
- [44] A. M. Fox, D. A. B. Miller, G. Livescu, J. E. Cunningham, and W. Y. Jan, “Excitonic effects in coupled quantum wells,” *Phys. Rev. B*, vol. 44, pp. 6231–6242, Sep 1991. [Online]. Available: <https://link.aps.org/doi/10.1103/PhysRevB.44.6231> (Cited on page 22.)
- [45] H. Shen, P. Parayanthal, F. Pollak, A. Smirl, J. Schulman, R. McFarlane, and I. D’Haenens, “Observation of symmetry forbidden transitions in the room temperature photoreflectance spectrum of a gaas/gaalas multiple quantum well,” *Solid State Communications*, vol. 59, no. 8, pp. 557–560, 1986. [Online]. Available: <https://www.sciencedirect.com/science/article/pii/003810988690058X> (Cited on page 22.)
- [46] H. Shen, X. C. Shen, F. H. Pollak, and R. N. Sacks, “Photoreflectance and photoreflectance-excitation spectroscopy of a gaas/ga_{0.67}al_{0.33}as multiple-quantum-well structure,” *Phys. Rev. B*, vol. 36, pp. 3487–3490, Aug 1987. [Online]. Available: <https://link.aps.org/doi/10.1103/PhysRevB.36.3487> (Cited on page 22.)
- [47] Z. M. Fang, A. Persson, and R. M. Cohen, “Allowed 3h-1e transition in semiconductor quantum wells,” *Phys. Rev. B*, vol. 37, pp. 4071–4075, Mar 1988. [Online]. Available: <https://link.aps.org/doi/10.1103/PhysRevB.37.4071> (Cited on page 22.)
- [48] G. Bastard, E. E. Mendez, L. L. Chang, and L. Esaki, “Exciton binding energy in quantum wells,” *Phys. Rev. B*, vol. 26, pp. 1974–1979, Aug 1982. [Online]. Available: <https://link.aps.org/doi/10.1103/PhysRevB.26.1974> (Cited on page 24.)
- [49] Y. Shinozuka and M. Matsuura, “Wannier exciton in quantum wells,” *Phys. Rev. B*, vol. 28, pp. 4878–4881, Oct 1983. [Online]. Available: <https://link.aps.org/doi/10.1103/PhysRevB.28.4878> (Cited on page 24.)
- [50] K. Kheng, R. T. Cox, M. Y. d’ Aubigné, F. Bassani, K. Saminadayar, and S. Tatarenko, “Observation of negatively charged excitons x^- in semiconductor quantum wells,” *Phys. Rev. Lett.*, vol. 71, pp. 1752–1755, Sep 1993. [Online]. Available: <https://link.aps.org/doi/10.1103/PhysRevLett.71.1752> (Cited on pages 24 and 27.)
- [51] M. A. Lampert, “Mobile and immobile effective-mass-particle complexes in nonmetallic solids,” *Phys. Rev. Lett.*, vol. 1, pp. 450–453, Dec 1958. [Online]. Available: <https://link.aps.org/doi/10.1103/PhysRevLett.1.450> (Cited on page 24.)
- [52] B. Stébé and A. Ainane, “Ground state energy and optical absorption of excitonic trions in two dimensional semiconductors,” *Superlattices and Microstructures*, vol. 5, no. 4, pp. 545–548, 1989. [Online]. Available:

- <https://www.sciencedirect.com/science/article/pii/0749603689903820> (Cited on page 24.)
- [53] P. Aceituno and A. Hernández-Cabrera, “The role of excitons and trions on electron spin polarization in quantum wells,” *Journal of Applied Physics*, vol. 110, no. 1, p. 013724, 2011. [Online]. Available: <https://doi.org/10.1063/1.3603031> (Cited on page 25.)
- [54] A. Manassen, E. Cohen, A. Ron, E. Linder, and L. N. Pfeiffer, “Exciton and trion spectral line shape in the presence of an electron gas in gaas/AlAs quantum wells,” *Phys. Rev. B*, vol. 54, pp. 10 609–10 613, Oct 1996. [Online]. Available: <https://link.aps.org/doi/10.1103/PhysRevB.54.10609> (Cited on pages 26 and 27.)
- [55] G. Finkelstein, H. Shtrikman, and I. Bar-Joseph, “Negatively and positively charged excitons in GaAs/Al_xGa_{1-x}As quantum wells,” *Phys. Rev. B*, vol. 53, pp. R1709–R1712, Jan 1996. [Online]. Available: <https://link.aps.org/doi/10.1103/PhysRevB.53.R1709> (Cited on pages 26 and 27.)
- [56] N. N. Sibeldin, M. L. Skorikov, and V. A. Tsvetkov, “Formation of charged excitonic complexes in shallow quantum wells of undoped GaAs/AlGaAs structures under below-barrier and above-barrier photoexcitation,” *Nanotechnology*, vol. 12, no. 4, pp. 591–596, nov 2001. [Online]. Available: <https://doi.org/10.1088/0957-4484/12/4/344> (Cited on page 27.)
- [57] I. Bar-Joseph, “Trions in GaAs quantum wells,” *Semiconductor Science and Technology*, vol. 20, no. 6, pp. R29–R39, may 2005. [Online]. Available: <https://doi.org/10.1088/0268-1242/20/6/r01> (Cited on page 27.)
- [58] C. Jirauschek and T. Kubis, “Modeling techniques for quantum cascade lasers,” *Applied Physics Reviews*, vol. 1, no. 1, p. 011307, 2014. [Online]. Available: <https://doi.org/10.1063/1.4863665> (Cited on pages 27 and 28.)
- [59] P. Harrison and A. Valavanis, *Numerical solutions*. John Wiley & Sons, Ltd, 2016, ch. 3, pp. 81–130. (Cited on page 27.)
- [60] L. R. Ram-Mohan, K. H. Yoo, and J. Moussa, “The Schrödinger–Poisson self-consistency in layered quantum semiconductor structures,” *Journal of Applied Physics*, vol. 95, no. 6, pp. 3081–3092, 2004. [Online]. Available: <https://doi.org/10.1063/1.1649458> (Cited on page 27.)
- [61] E. Cassan, “On the reduction of direct tunneling leakage through ultrathin gate oxides by a one-dimensional Schrödinger–Poisson solver,” *Journal of Applied Physics*, vol. 87, no. 11, pp. 7931–7939, 2000. [Online]. Available: <https://doi.org/10.1063/1.373477> (Cited on page 27.)

- [62] Y. Ando and T. Itoh, “Calculation of transmission tunneling current across arbitrary potential barriers,” *Journal of Applied Physics*, vol. 61, no. 4, pp. 1497–1502, 1987. [Online]. Available: <https://doi.org/10.1063/1.338082> (Cited on page 27.)
- [63] G. Bastard, *Wave mechanics applied to semiconductor heterostructures*. Wiley, 1990. (Cited on page 27.)
- [64] V. D. Jovanović, D. Indjin, N. Vukmirović, Z. Ikonić, P. Harrison, E. H. Linfield, H. Page, X. Marcadet, C. Sirtori, C. Worrall, H. E. Beere, and D. A. Ritchie, “Mechanisms of dynamic range limitations in GaAs/AlGaAs quantum-cascade lasers: Influence of injector doping,” *Applied Physics Letters*, vol. 86, no. 21, p. 211117, 2005. [Online]. Available: <https://doi.org/10.1063/1.1937993> (Cited on page 28.)
- [65] A. Lastras-Martínez, R. E. Balderas-Navarro, L. F. Lastras-Martínez, and M. A. Vidal, “Model for the linear electro-optic reflectance-difference spectrum of gaas(001) around E_1 and $E_1 + \Delta_1$,” *Phys. Rev. B*, vol. 59, pp. 10 234–10 239, Apr 1999. [Online]. Available: <https://link.aps.org/doi/10.1103/PhysRevB.59.10234> (Cited on page 29.)
- [66] D. E. Aspnes and A. A. Studna, “Anisotropies in the above-band-gap optical spectra of cubic semiconductors,” *Phys. Rev. Lett.*, vol. 54, pp. 1956–1959, Apr 1985. [Online]. Available: <https://link.aps.org/doi/10.1103/PhysRevLett.54.1956> (Cited on page 30.)
- [67] D. E. Aspnes, “Above-bandgap optical anisotropies in cubic semiconductors: A visible–near ultraviolet probe of surfaces,” *Journal of Vacuum Science & Technology B: Microelectronics Processing and Phenomena*, vol. 3, no. 5, pp. 1498–1506, 1985. [Online]. Available: <https://avs.scitation.org/doi/abs/10.1116/1.582974> (Cited on page 30.)
- [68] S.-H. Wei and A. Zunger, “Theory of reflectance-difference spectroscopy in ordered iii-v semiconductor alloys,” *Phys. Rev. B*, vol. 51, pp. 14 110–14 114, May 1995. [Online]. Available: <https://link.aps.org/doi/10.1103/PhysRevB.51.14110> (Cited on page 30.)
- [69] L. F. Lastras-Martínez, A. Lastras-Martínez, and R. E. Balderas-Navarro, “A spectrometer for the measurement of reflectance-difference spectra,” *Review of Scientific Instruments*, vol. 64, no. 8, pp. 2147–2152, 1993. (Cited on page 30.)
- [70] B. Koopmans, B. Koopmans, P. Santos, P. Santos, and M. Cardona, “Microscopic reflection difference spectroscopy on semiconductor nanostructures,” *physica status solidi (a)*, vol. 170, no. 2, pp. 307–315, 1998. (Cited on page 30.)
- [71] Y. H. Chen, X. L. Ye, J. Z. Wang, Z. G. Wang, and Z. Yang, “Interface-related in-plane optical anisotropy in gaas/al_xga_{1-x}As single-quantum-well structures studied by reflectance difference spectroscopy,” *Phys. Rev. B*, vol. 66, p. 195321, Nov 2002. (Cited on page 34.)

- [72] R. Winkler, *Spin-orbit coupling effects in two-dimensional electron and hole systems*. Springer, 2003, vol. 191. (Cited on page 36.)